Numerical Simulation of High Energy Density Plasmas in Support of KALIF Experiments

J.J. MacFarlane, P. Wang, D.L. Henderson, O. Yasar

January 1993

UWFDM-910

FUSION TECHNOLOGY INSTITUTE

UNIVERSITY OF WISCONSIN

MADISON WISCONSIN

Numerical Simulation of High Energy Density Plasmas in Support of KALIF Experiments

J.J. MacFarlane, P. Wang, D.L. Henderson, O. Yasar

Fusion Technology Institute
University of Wisconsin
1500 Engineering Drive
Madison, WI 53706

http://fti.neep.wisc.edu

January 1993

UWFDM-910

Contents

Appendix C

Aluminum K_α Line Emissison as a Diagnostic in Light Ion Beam Fusion Experiments

Appendix D

Thermal Ionization Effects on Inner-Shell Line Emission for Au Targets Heated by Intense Light Ion Beams

Appendix E

Theoretical Spectroscopic Analysis of Intense Ion Beam-Plasma Interaction in the PBFA-II Gas Cell

1. Introduction

The purpose of this report is to provide a detailed description of work performed during the 1992 calendar year in the areas of spectral diagnostic analysis and radiation-hydrodynamics modeling for light ion beam-heated plasmas. This work has been supported by Kernforschungszentrum Karlsruhe (KfK) as part of a multiyear effort to develop theoretical models and computational tools which can be used to study high energy density plasmas created by KALIF (the Karlsruhe Light Ion Facility). To date, we have developed and tested a collisional-radiative equilibrium (CRE) code in which multilevel atomic rate equations can be solved self-consistently with the radiation field and ion beam properties. In addition, a suite of atomic physics codes has been put together to generate a high quality atomic physics data base which is used by the CRE code. We have also recently coupled major portions of the CRE code into KATACO in order to allow for more accurate treatment of line transport effects. Finally, several series of calculations were performed over the course of our work with KfK to provide theoretical diagnostics support for KALIF experiments.

The tasks performed for our 1992 contract with KfK are listed in Table 1.1. The first task was to perform CRE and atomic physics calculations in support of KALIF experiments. In addition to the Al K_α analyses described in Appendices A, B, and C, we have performed calculations to investigate the sensitivity of oxygen K_α emission and absorption spectra to the target plasma temperature and density. Oxygen was chosen because its satellites show much greater temperature sensitivity in the 2 to 20 eV temperature range. This work is summarized in Section 2.

Tasks 2 and 3 involved coupling the CRE code (NLTERT) with KATACO, and installing it along with the standalone CRE and supporting atomic physics codes on the KfK computers. Details of this work are provided in Section 3.

We have also performed a brief analysis of hydrogen Balmer line opacities in support of diode plasma experiments being performed by H. Laqua and H. Bluhm. This work is summarized in Section 4.

Finally, the appendices of this report contain a series of papers written by the authors during the past year which describe investigations on diagnostics analyses for light ion beam experiments. Although some of the work was supported by the Particle Beam Fusion Accelerator (PBFA-II) program at Sandia National Laboratories, much of it is applicable to future KALIF experiments. Appendices A through C concern our Al K_α

Table 1.1. Tasks for 1992

1. Perform collisional-radiative equilibrium simulations to develop a conceptual target design for a KALIF beam/plasma interaction experiment.
   - **(a)** Perform multicomponent plasma calculations for layered targets.
   - **(b)** Perform supporting atomic physics calculations.
   - **(c)** Predict spectral fluxes and optimum spectral ranges for determining plasma temperature.
2. Couple the non-LTE radiative transfer code NLTERT with KATACO/MEDUSA.
   - **(a)** Obtain a working version of KATACO that has been tested on a KfK workstation. Implement on workstation at Wisconsin.
   - **(b)** Implement radiation/plasma energy coupling model.
3. Install KATACO/NLTERT and standalone NLTERT, and supporting atomic physics codes at KfK.
4. Document results in a final report to KfK.

analyses for diagnosing plasma conditions in light ion beam experiments. In Appendix D, results are presented from our investigation of the ionization dependence of atomic quantities which affect Au inner-shell line radiation. Finally, Appendix E describes our analysis of visible line emission spectra obtained from the gas cell region in PBFA-II experiments.

2. Diagnosing Target Plasma Conditions Using K_α Line Radiation

During the past year, we have continued to investigate the use of K_α line radiation from moderate-Z plasmas as a method for diagnosing conditions in targets heated by intense proton beams. This work was concentrated in four areas. First, to further test the reliability of our physics models we compared results of our calculations with an Al K_α absorption spectrum obtained in a laser-produced plasma experiment performed at Lawrence Livermore National Laboratories (Perry et al. 1991). Our results were found to be in very good agreement both with the experimental spectrum and the calculated spectrum of Abdallah et al. (1991; Perry et al. 1991). Second, we performed a series of calculations to study the dependence of Al K_α spectra on the temperature, density, and thickness of the diagnostic layer. These results were presented at the Ninth Topical Conference on High-Temperature Plasma Diagnostics in Santa Fe, NM, in March 1992 (MacFarlane et al. 1992). The corresponding paper appears in Appendix C of this report. Third, we have completed our analysis of the K_α emission spectrum obtained in the Sandia PBFA-II experiment reported by Bailey et al. (1990). This collaborative effort included contributions from T. Mehlhorn, J. Bailey, and R. Dukart of Sandia and R. Mancini at the University of Florida. Work completed this year included examining in detail the role of excited states in the production of K_α satellite spectra and the density sensitivity of lines originating from both ground state and excited state configurations. This work has been accepted for publication in Physical Review (MacFarlane et al. 1993). The final manuscript appears in Appendix A. A detailed description of the supporting atomic physics calculations has been prepared for publication (Wang et al. 1993). This appears in Appendix B. Finally, we have performed a series of calculations to examine the possibility of using oxygen K_α satellites as a diagnostic for moderate temperature plasmas ($T \simeq 2$ - 20 eV). These results are presented later in this section.

2.1. K_α Absorption Spectroscopy: Comparison Between Theory and Experiment

Results from an opacity measurement experiment in which a K_α absorption spectrum was measured for a well characterized Al plasma were recently published by Perry et al. (1991). The experiments were performed using the NOVA laser system at Lawrence Livermore National Laboratory. In this experiment, a target consisting of Al foils (with thicknesses of 500 and 1500 Å) sandwiched within a 2 μm-thick plastic slab

was irradiated by a high intensity laser. The plastic was used to tamp the foil expansion and produce a more uniform density in the Al. A foil temperature of 58 eV and density of 0.020 g/cm^3 were independently measured in separate shots. A separate beam was used to heat a samarium x-ray backlighter.

Figure 2.1 shows the absorption spectrum obtained by Perry et al. for the 500 Å-thick Al foil. The dark line represents the experimental spectrum while the faint line represents the spectrum calculated by that group using a temperature of 58 eV and density of 0.020 g/cm^3. A FWHM of 0.6 eV was assumed for the calculated line widths, which was determined from the spectral resolution of the detector. The agreement between theory and experiment is quite good.

To test the reliability of our physics models we performed calculations for the same conditions as those reported in Perry et al. Our results are shown in Figure 2.2. The line widths were adjusted to account for the 0.6 eV (FWHM) spectral resolution of the detector. We find our calculations are also in good agreement with the experimental absorption spectrum. In some ways, this represents a more stringent test for our models than the Sandia K_α spectrum reported by Bailey et al. (1990) because: (1) the thin layers used in the LLNL experiment mitigate problems associated with excessive opacity effects, and (2) the time-resolved measurement allows for a more well-defined temperature and density.

We performed several additional calculations to investigate the sensitivity of the K_α absorption spectrum to changes in temperature and density. Results are shown in Figure 2.3. The top plot shows the spectrum computed for $T = 58$ eV, $\rho = 0.020$ g/cm^3, and a pre-expansion thickness of $L_{orig} = 500$ Å. The bottom spectrum was computed for the same conditions with the exception that the temperature was $T = 53$ eV (i.e., about 10% lower). Note that the He-like feature disappears at this lower temperature while the C-like features are much more pronounced. The middle plot shows the spectrum computed for $T = 58$ eV, $\rho = 0.004$ g/cm^3, and $L_{orig} = 500$ Å. The factor of 5 decrease in density leads to a readily observable shift to higher ionization stage.

The sensitivity of the K_α satellite spectrum to temperature and density suggests it can be a valuable diagnostic for determining target plasma conditions. If time-resolved emission spectra using thin tracer layers ($L_{orig} \sim 10^3$ Å) could be obtained from proton beam–plasma interaction experiments, it is felt that target plasma conditions could be diagnosed with reasonably good accuracy using the K_α technique. Since *emission* spectra

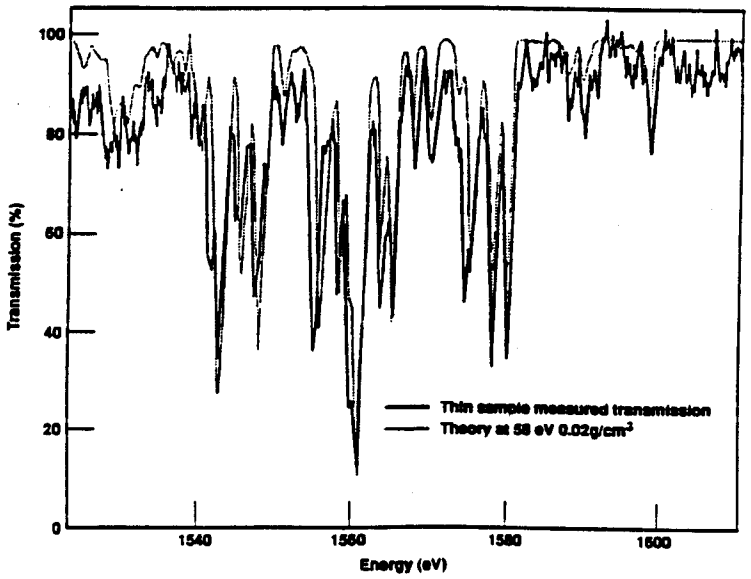

Figure 2.1. Aluminum K_α absorption spectrum measured by Perry et al. (1991) for a 500 Å thick Al foil. The dotted line represents the calculation by Abdallah et al. for a foil at $T = 58$ eV and $\rho = 0.02$ g/cm^3.

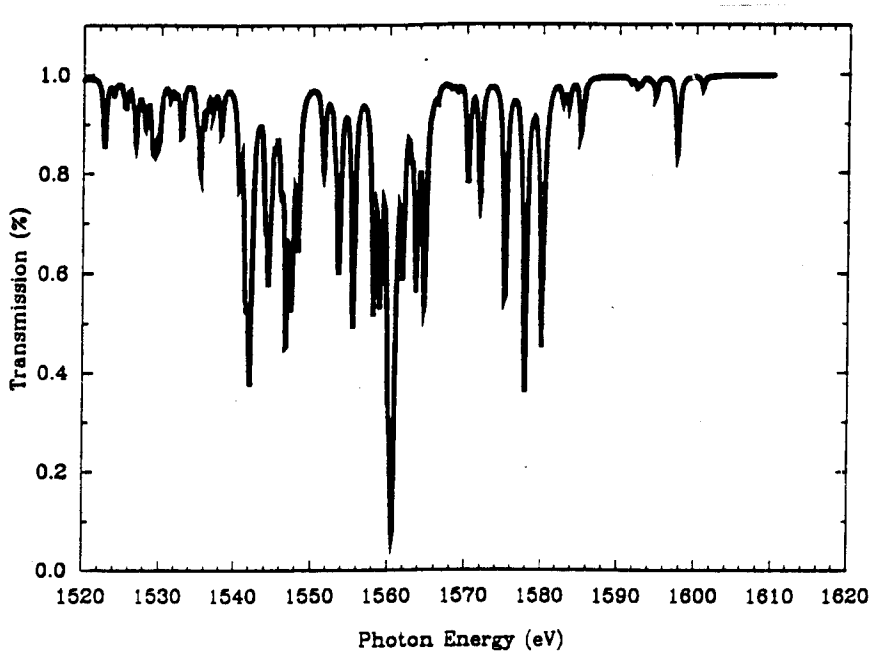

Figure 2.2. Our calculated Al K_α absorption spectrum for the same plasma conditions as Figure 2.1. Note the good agreement between theory and experiment.

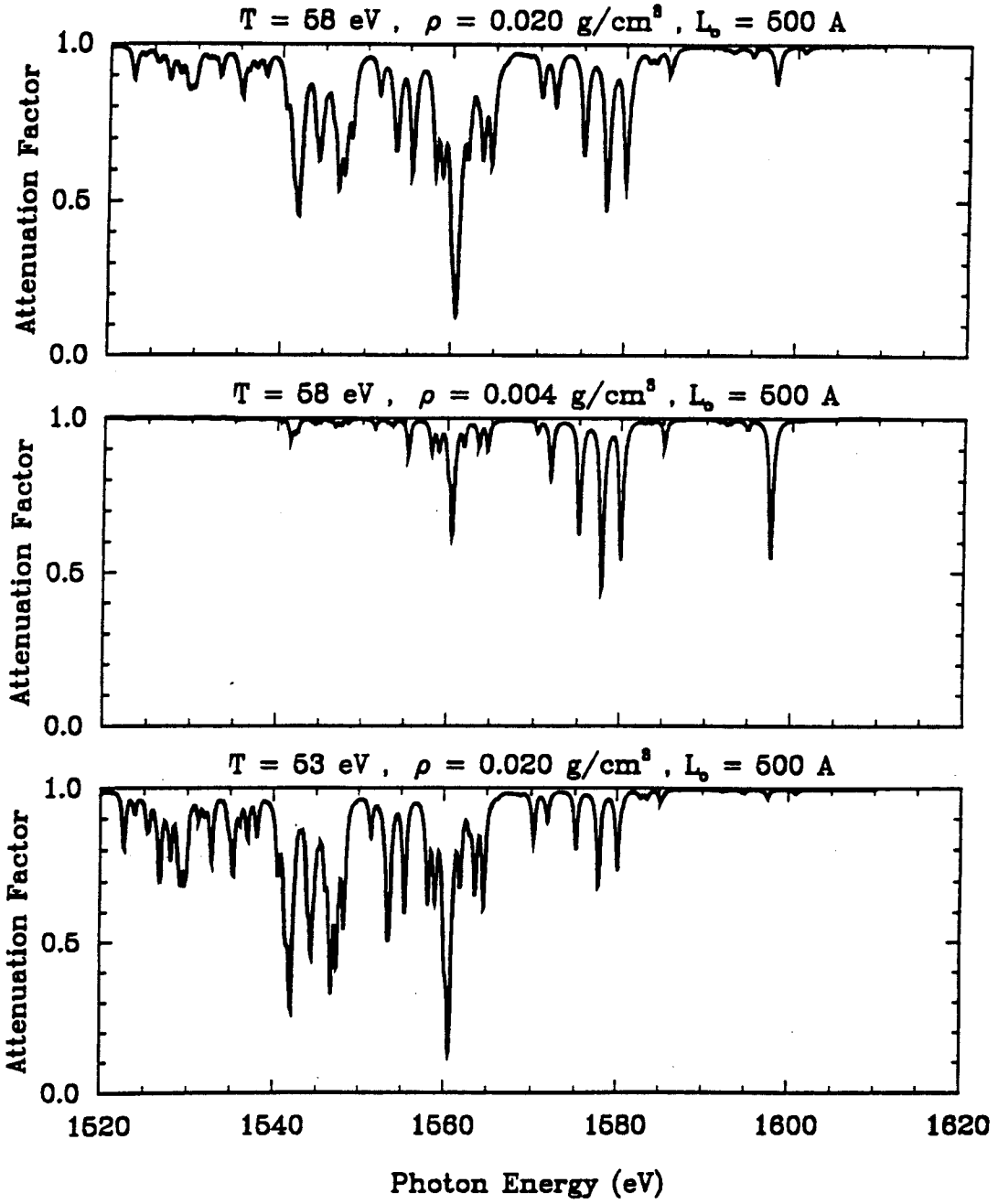

Figure 2.3. Sensitivity of Al K_α absorption spectrum to temperature and density. Spectra were calculated for $\rho L = \rho_{solid} \cdot 500\,\text{Å}$ with: (top) $T = 58$ eV and $\rho = 0.020\,\text{g/cm}^3$; (middle) $T = 58$ eV and $\rho = 0.004\,\text{g/cm}^3$; (bottom) $T = 53$ eV and $\rho = 0.020\,\text{g/cm}^3$.

are a natural occurrence in light ion beam experiments because the beam creates K-shell vacancies in the target plasma, absorption spectroscopy using an x-ray backlighter is not required to determine plasma conditions. (It is also interesting to note that K_α emission lines have been observed in laser-produced plasmas (Soom 1992) due to the presence of "hot" electrons.)

2.2. Oxygen K_α Line Emission as a Diagnostic in Moderate Temperature Plasmas Created by an Intense Proton Beam

Previous investigation of Al K_α line emission has shown it to be a potentially valuable diagnostic in light ion beam-plasma interaction experiments for plasmas in the range of 15 –100 eV. At lower temperatures, blue-shifted satellite lines (see Appendix A) are not observed because the L-shell remains filled. This means that the Al K_α diagnostic technique does not provide a good method for determining temperatures at $T \lesssim 10$ eV. A better element for diagnosing temperatures in the $2 \lesssim T \lesssim 20$ eV range is oxygen. Since oxygen always has L-shell vacancies, K_α satellites for all ionization stages exhibit a significant shift in wavelength, and therefore provide a good means of measuring the ionization distribution and, from that, plasma conditions. (The same arguments apply for elements of similar atomic number; e.g., N through Ne.)

One possible application of such a diagnostic would be in KALIF beam-target interaction experiments performed using the B_θ diode. Since typical power densities achieved using the B_θ diode are $\sim 0.2 - 0.3$ TW/cm^2, one expects the temperatures in the target to be $\sim 5 - 20$ eV (Goel 1992). Let us then consider the case of the KALIF shock wave experiments.

We consider the case illustrated in Figure 2.4, where a proton beam deposits its energy in a thin ($\sim 20\,\mu$m) Al ablator, which subsequently drives a strong shock into a thick layer ($\sim 0.1 - 1$ cm) of material such as LiF. As the Al layer absorbs the ion beam energy it rapidly vaporizes and expands. One way to determine the conditions in the ablator region is to implant a thin diagnostic tracer layer ($\Delta L \sim 1000$ Å) composed of oxygen (or some oxidized compound). If this could be done one could determine the plasma conditions at the location of the tracer layer by measuring the K_α emission spectrum from the O layer. In the remainder of this section we show the sensitivity of the K_α spectrum to temperature and density, and discuss the effects of opacity in such an experiment.

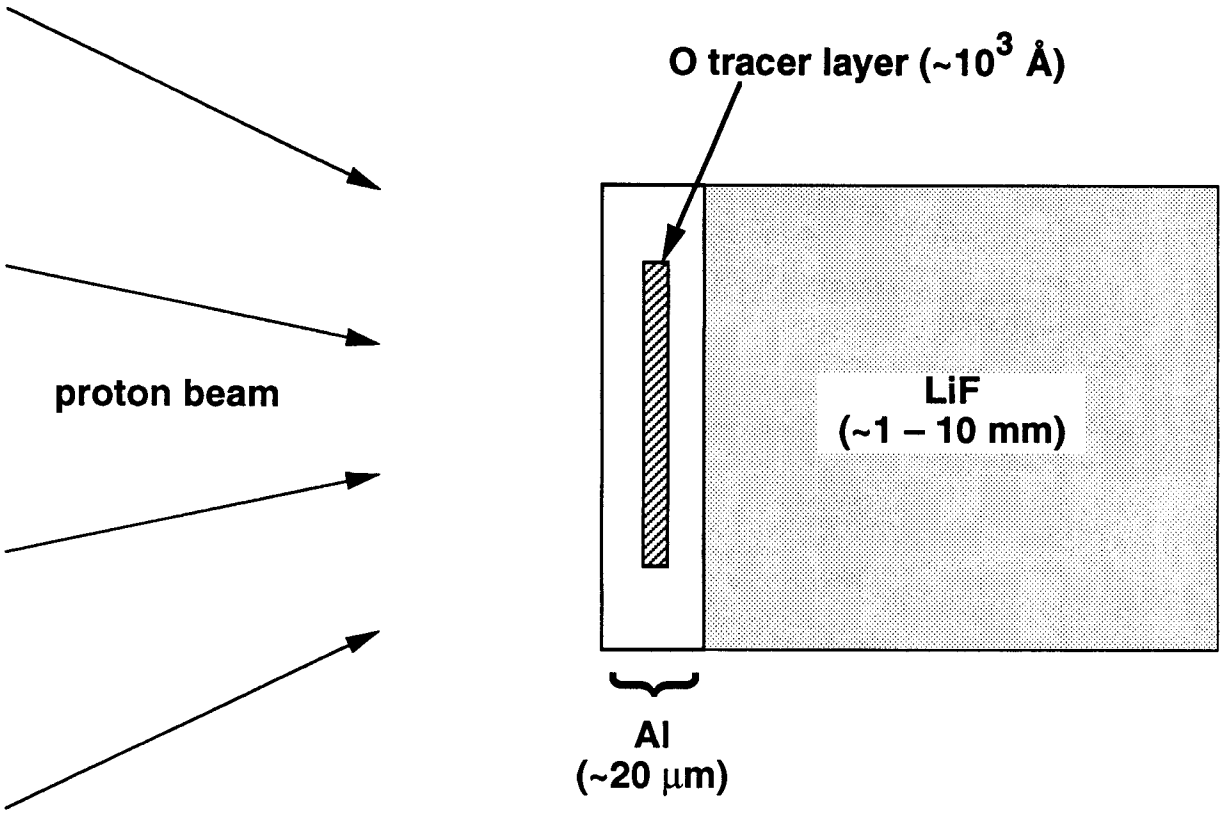

Figure 2.4. Schematic illustration of the placement of an oxygen diagnostic tracer layer in a shock wave experiment. The purpose of the tracer would be to determine the plasma conditions at some point within the ablator region.

To compute the O K_α spectrum we have used CRE and atomic physics codes which are described elsewhere (see Appendices). The incident proton beam is assumed to have a power density of 0.25 TW/cm^2, and proton energies of about 1.5 MeV. At this energy the proton impact ionization cross section for O K-shell electrons is about 2.2×10^{19} cm^2. Figure 2.5 shows the dependence of the cross section on the incident proton energy calculated using a plane wave Born approximation (PWBA) model. Note that the cross section peaks at $E_p \approx 1.0$ – 1.5 MeV. For the assumed beam conditions, the K-shell vacancy creation rate is 2.3×10^5 transitions/s/target ion.

Calculations were performed for oxygen plasma temperatures ranging from 2 to 20 eV and densities ranging from 10^{-3} to $10^{-1}\, n_o$ ($n_o \equiv$ solid density). In our calculations we use a model atom for O consisting of 494 levels distributed over all 9 ionization stages. The thickness of 1000 Å unless otherwise noted. (Thus at $n = 10^{-2}\, n_o$, the thickness was 10^5 Å $= 10\ \mu$m.) A fluorescence yield of 0.0083 was assumed for all O ions (Krause 1979).

Figure 2.6 shows the sensitivity of the O K_α satellite spectrum to temperature. Results are shown from calculations at $T = 2$, 5, 10, and 20 eV. In each case the density was $n = 10^{-2}\, n_o$. At 2 eV, line emission from O I (recall this is O II after proton impact ionization) dominates the spectrum. At 5 eV, K_α satellites from O II exhibit the strongest fluxes. O III and O IV lines dominate at 10 eV, while those from O V are seen at $T = 20$ eV. Thus, over the entire range shown there is very good sensitivity to the temperature.

The corresponding absorption spectra are shown in Figure 2.7. These represent spectra that could be observed if an x-ray backlighter were placed on the side of the target opposite the detector. At $T = 2$ eV (bottom) O I lines produce the greatest absorption. K-shell bound-free absorption edges are also readily seen in the figure. At higher temperatures, absorption is due to higher degrees of ionization (as discussed for Figure 2.6).

Note that a target with an areal density ($\equiv n \cdot \Delta L$) of $\sim 10^{17} - 10^{18}$cm^{-2} (or $\sim 0.1\,\mu$m at solid density) is a good thickness for both emission and absorption spectroscopy. It is good for absorption spectroscopy because the optical depths of strong lines are $\sim 10^0 - 10^1$ at line center. If the optical depths were significantly greater the absorption spectrum can become saturated. If they were significantly less little absorption would occur. In the case of emission spectroscopy, one wants the diagnostic layer to be thick enough to produce a sufficient flux at the detector, but thin enough that resonant

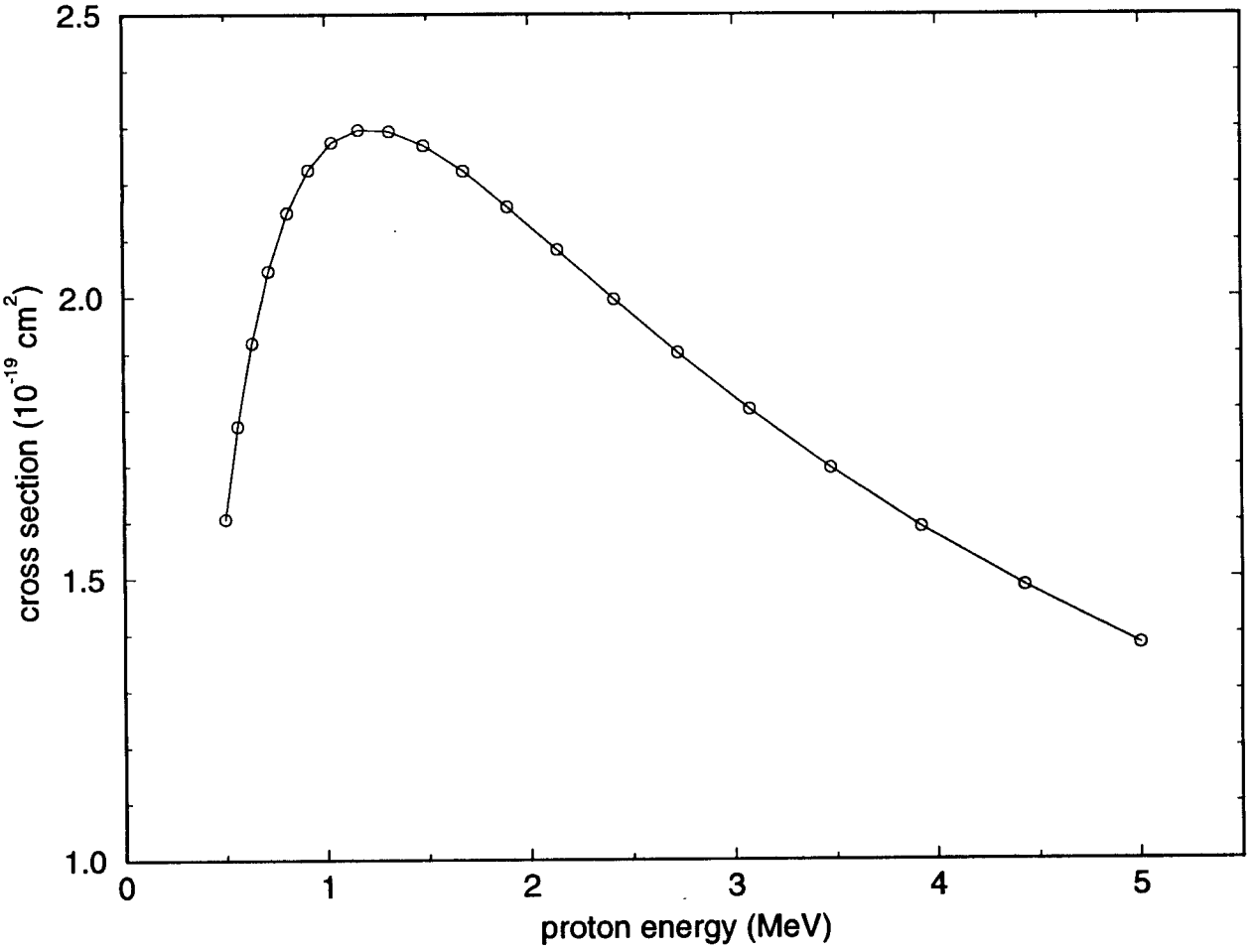

Figure 2.5. Calculated proton impact ionization cross section for K-shell electrons of O II as a function of the incident proton energy.

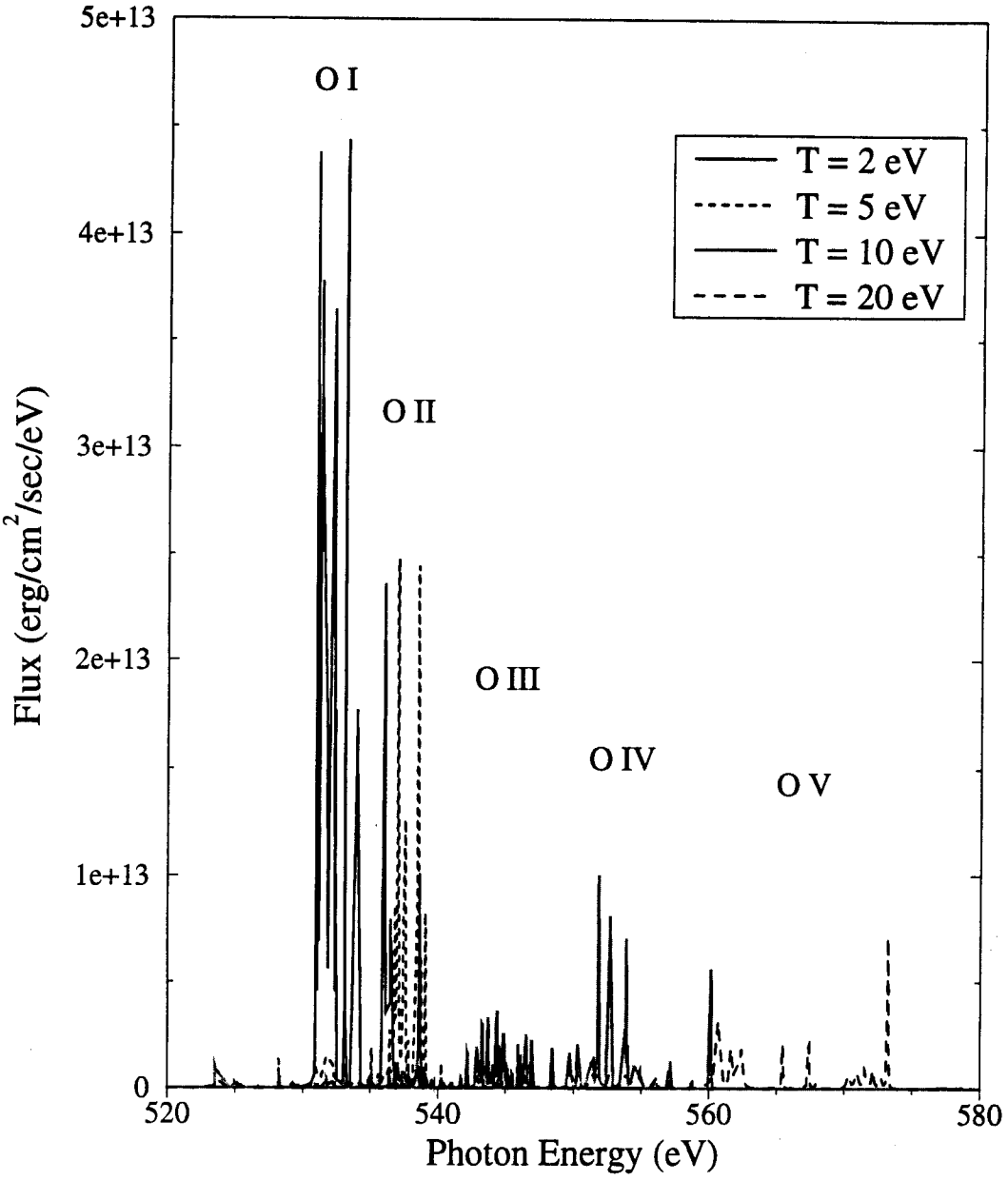

Figure 2.6. Oxygen K_α emission spectra for plasma temperatures of 2, 5, 10, and 20 eV. In each case the density is $10^{-2}\, n_o$ and the tracer layer (solid density) thickness is 1000 Å. Note the significant shift to higher energies and ionization stage as the temperature increases.

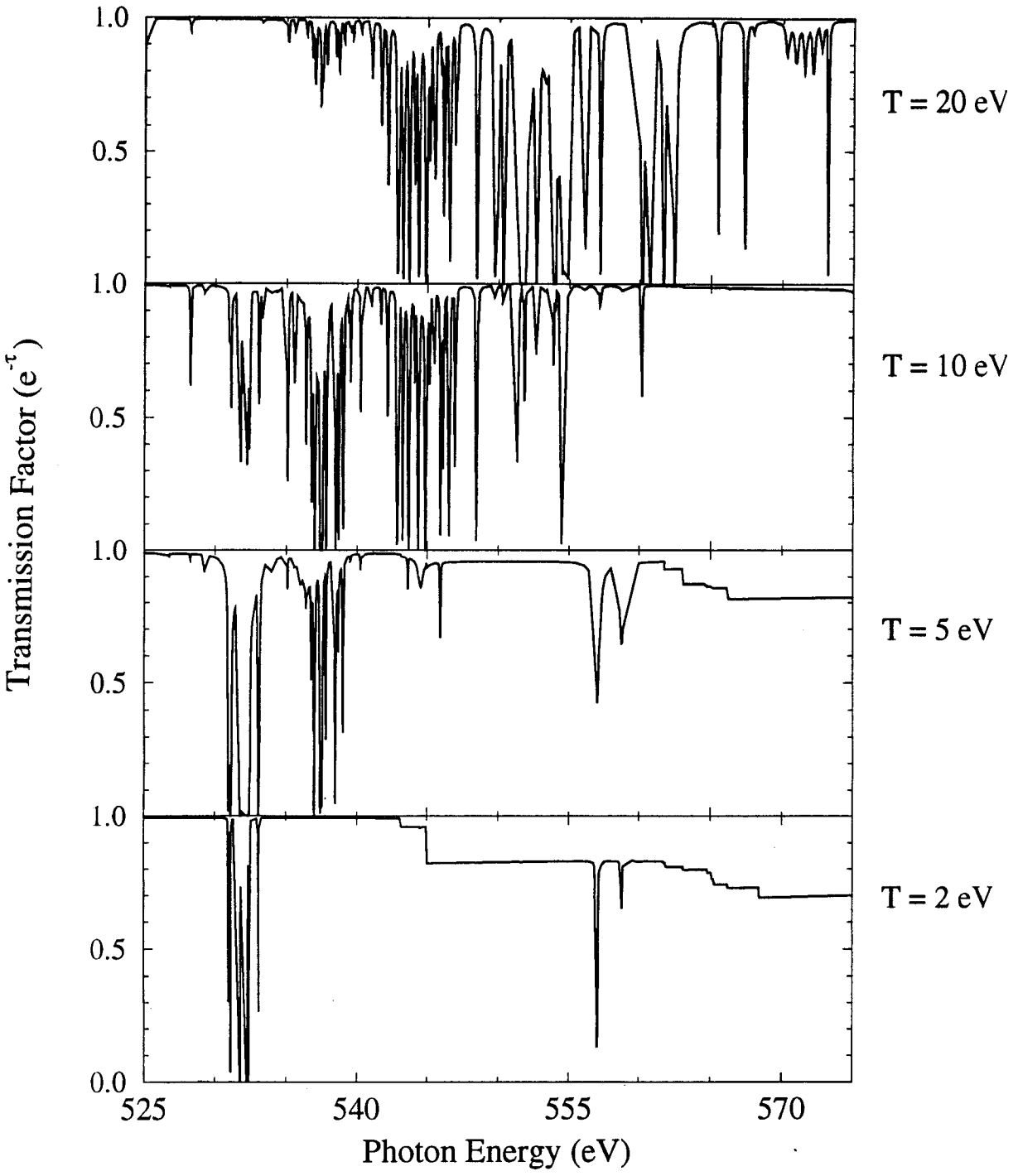

Figure 2.7. Oxygen K_α absorption spectra for the same plasma conditions as those in Figure 2.6. Note that tracer thicknesses $\sim 10^3$ Å are optimum for absorption spectroscopy for the K_α satellite spectral region.

self-absorption does not skew the resultant spectrum significantly (see Appendix A). Thus $n \cdot \Delta L \sim 10^{17} - 10^{18}\,\mathrm{cm}^{-2}$ should represent a good compromise in this regard.

Figure 2.8 shows the sensitivity of the emission spectrum to density. In each calculation the temperature was 10 eV, while the areal density was 1000 Å $\cdot\, n_o$. Thus, this can be viewed as the spectrum observed from a planar foil that has expanded $10^1, 10^2$, and 10^3 times. At lower densities, K_α emission is strongest from lines of relatively high ionization stage. This of course results from the fact that 3-body (collisional) recombination is the dominant recombination process. As the density increases, not only does the mean ionization state decrease but the lines become noticeably thicker due to Stark broadening.

Finally, the optical depth of the K_α spectral region is shown in Figure 2.9 for oxygen layers of 2 areal densities: $100\,\mu\mathrm{m} \cdot n_o$ and $0.1\,\mu\mathrm{m} \cdot n_o$. Note that in the 100 μm case the region is optically thick to both lines ($\tau_L \sim 10^3 - 10^4$) and continuum ($\tau_{cont} \sim 10^1$). On the other hand only the relatively strong lines are optically thick for the 0.1 μm case. Figure 2.9 also shows the K_β lines at $h\nu \gtrsim 570$ eV. These lines result for 3p – 1s transitions and therefore the emission lines can provide information about *excited* state populations for oxygen ions.

In designing targets for light ion beam experiments it is important to consider the effects of opacity of all materials. This is because the stopping range of light ions is relatively long (compared with laser or heavy ion energy deposition), and often dictates that the stopping medium be fairly thick ($\sim 10^1 - 10^2\,\mu$m). At these thicknesses many materials can be optically thick to soft x-rays.

To illustrate this point consider the target in Figure 2.4. The K_α emission from the O tracer layer can be absorbed by both the Al and LiF regions if the detector is placed at the right. The continuum absorption cross sections of the absorbing layers at the photon energy of the O K_α lines (about 0.55 keV) are:

Atom	$\sigma\,(\mathrm{cm}^2/\mathrm{g})$
Al L-shell	6.0×10^3
F L-shell	1.4×10^3
Li K-shell	1.3×10^3

This corresponds to optical depths of $\tau = 1.6$ per μm for the Al ablator and $\tau = 360$ per mm for the LiF region. Since the LiF region is typically several mm thick, virtually

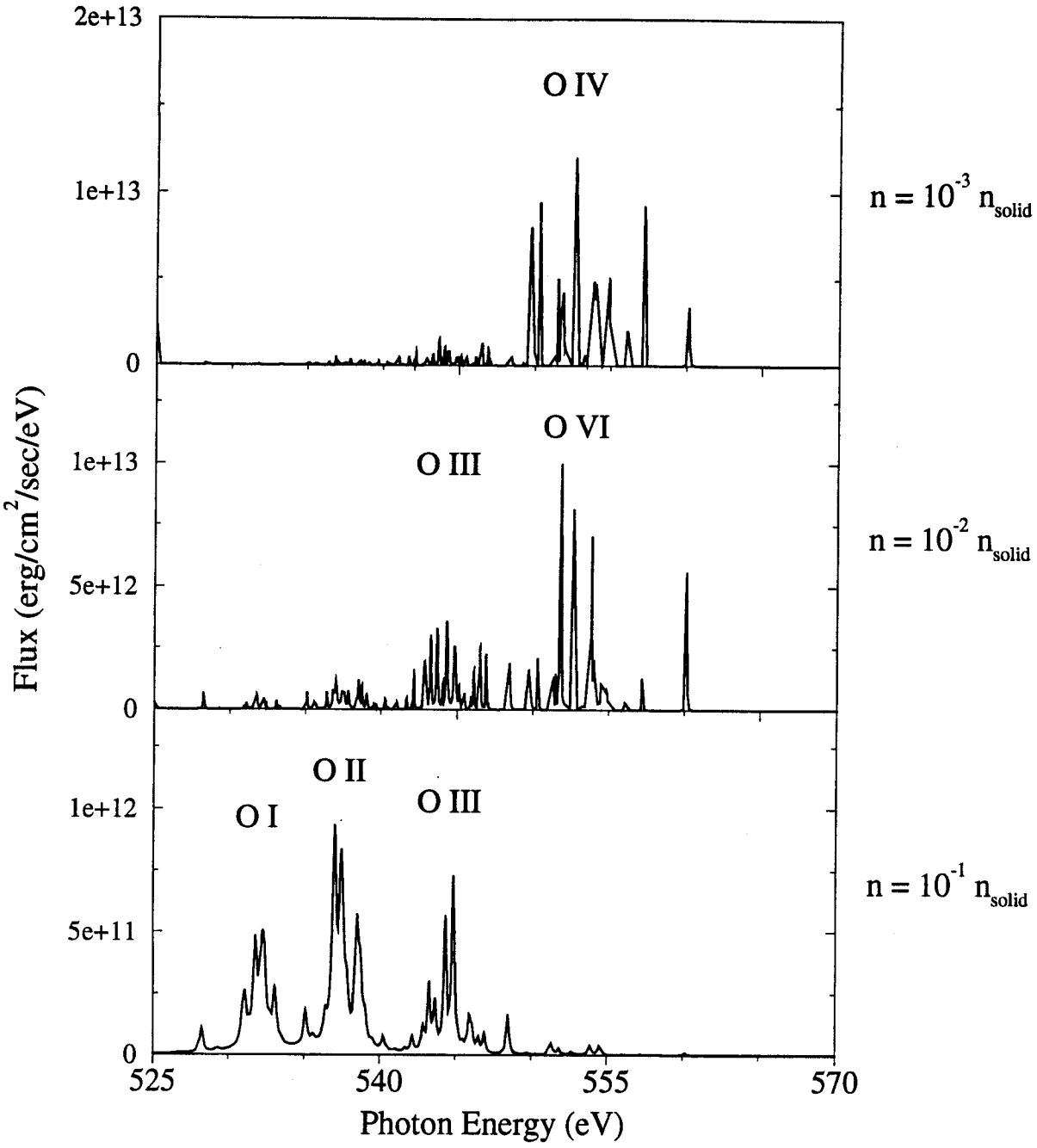

Figure 2.8. Dependence of oxygen K_α emission spectrum on density. In each case $T = 10$ eV and $L_{orig} = 1000$ Å. Note that the lines become significantly Stark-broadened at $n \gtrsim 10^{-1}\, n_o$.

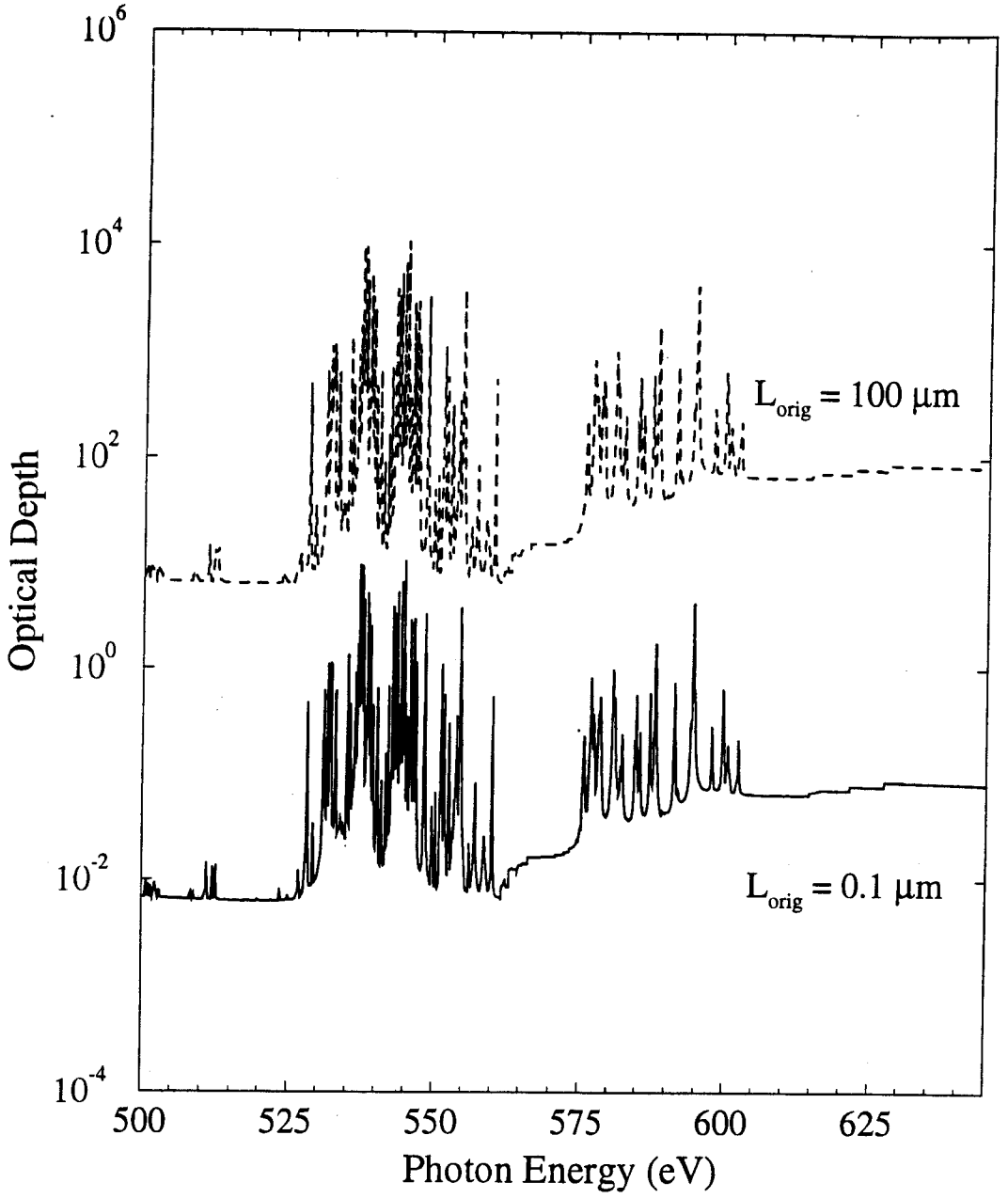

Figure 2.9. Optical depth as a function of photon energy in the O K_α and K_β spectral region. The solid and dashed curves correspond to tracer layer (pre-expansion) thicknesses of 0.1 μm and 100 μm, respectively. In each case $T = 10$ eV and $n = 10^{-2}\, n_o$.

no photons from the O tracer will pass through this region. O K_α photons will also be attenuated somewhat by the Al layer. However, this attentuation is not prohibitive if the photons have to pass through $\lesssim$ a few μm.

To observe the K_α photons from the tracer layer, the optical path from the source to the detector must be carefully chosen. Some possible ways to avoid attenuation by the LiF layer include:

(a) clear a window (hole) in the LiF so that photons can reach the detector;

(b) perform separate experiments without the LiF region; or

(c) position the detector on the beam side of the target so that it does not have to look through the LiF region.

In designing such an experiment, the trade-offs associated with each of these options must be carefully considered. For instance, in item (a) the hole should be small enough so that the measurement of the shock velocity is not affected, but large enough so that the flux from the O K_α lines can be measured. For item (b) good reproduceability from experiment to experiment must be possible. And for item (c), there must be sufficient room on the diode side of the target to place the detector. Final design recommendations for this type of experiment should therefore be based on the minimum flux needed for the x-ray detector, target/driver orientation, shot-to-shot reproduceability, and so forth.

In summary, the K_α diagnostic technique can be used to determine conditions for relatively low temperature plasmas using tracers with $Z \approx 8$. Thin tracer layers with thicknesses $\sim 10^2 - 10^3$ Å are best because they mitigate opacity effects. Attenuation of K_α photons emitted from the tracer layer by overlying material can be signifiant, so the optical path to the x-ray detector must be carefully chosen.

3. Code Development and Implementation

During the past year, we have integrated the CRE model into MULRAD, the multigroup radiation diffusion version of KATACO. This will allow for more accurate simulation of the dynamics of high energy density plasmas, particularly in cases where the plasma is optically thick to line radiation while being optically thin to continuum radiation. This code has been installed on the IBM mainframe at KfK. In addition we have installed standalone versions of our CRE code and supporting atomic physics codes on the IBM mainframe and STARDENT workstation at KfK.

In this section we provide a brief description of the procedure one follows to run the atomic physics codes and CRE code in Sections 3.1 and 3.2, respectively. In Section 3.3, we describe the coupling of the CRE algorithms with KATACO.

3.1. Atomic Physics Data Calculation Package

This section describes how detailed atomic data are calculated using our atomic physics codes, and how this atomic data is interfaced with the CRE and KATACO-CRE codes.

Our atomic physics calculation package consists of four modules:

1. ATBASE computes atomic structure and radiative data. It is used to calculate atomic energy levels, oscillator strengths, and photoionization cross sections. In this code, Hartree-Fock radial functions are used to construct configuration-interaction (CI) wavefunctions. The intermediate coupling scheme employed determines fine structure energy levels and atomic spectral properties.

2. CPSSR calculates ion impact ionization cross sections. The plane-wave Born approximation — with corrections for polarization and binding effects, Coulomb deflection, and relativistic effects — is used for treating the collision process.

3. ATTABLE generates tabular data for an "atomic model" using output from ATBASE. It functions as an interface, calculating raw atomic physics data for the CRE and KATACO-CRE codes. It takes output from ATBASE, fills in the requested number of Rydberg energy levels based on a scaled hydrogenic approximation, and calculates collisional and radiative rate coefficients at several temperature and density points. The data tables output from this code are the atomic data files read into CRE and KATACO-CRE.

4. STATE is a "user friendly" module which generates input data files for ATBASE.

In creating an atomic model for a specific problem, two things are critical. The first is how to select the levels and the second is how to couple the levels. To date, the selection of energy levels is in some sense an "art" which must be based on physical insight, computing time requirements, and experience. For the energy level coupling, the default procedure using the modules described above generates tables in which dipole-allowed coupling is assumed. To generate models with more complete coupling between levels, data calculated with other codes are necessary. Such data files may be provided on request.

The atomic model data files generated for CRE and KATACO-CRE include data for the following processes:

- electron impact excitation/deexcitation (dipole-allowed)
- electron impact ionization/recombination
- spontaneous emission
- stimulated absorption/emission (oscillator strengths)
- photoionization/radiative recombination
- dielectronic recombination.

At present, ion beam impact ionization rate coefficients, which are determined from CPSSR (PWBA) calculations, must be supplied to the CRE code via its namelist input file.

Next, a simple operation guide is provided for the creation of an atomic model using STATE, ATBASE, ATTABLE, and CPSSR. A flow diagram illustrating the relation between the various modules is shown in Figure 3.1. In the figure and in the text below, the input/output file names will be referred to by their UNIX names.

3.1.1. STATE

For each ion of the atomic model (excluding H-like and fully ionized) STATE generates two files which are input to ATBASE. Input to STATE consists of two files containing information about energy level coupling for normal and autoionization

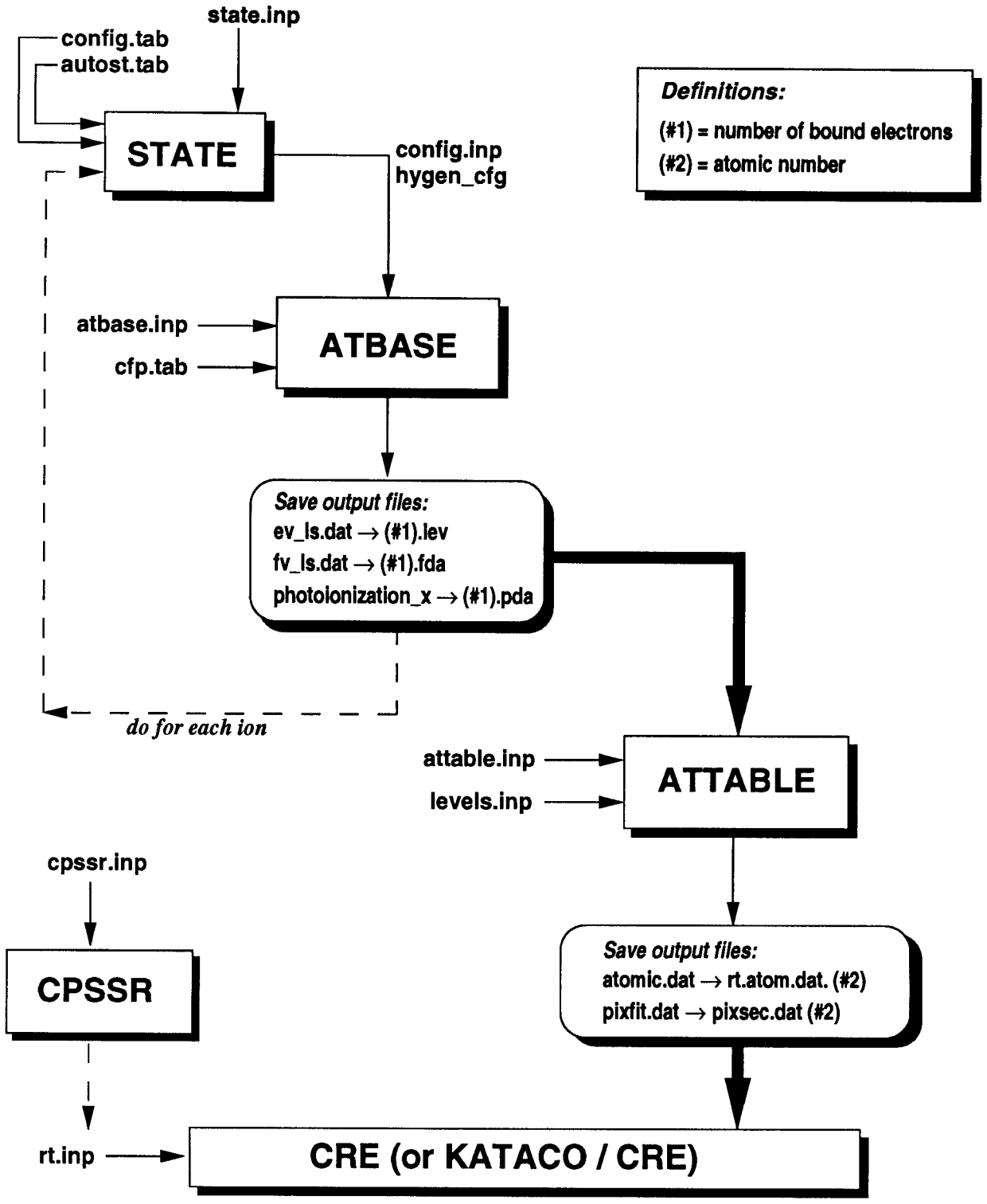

Figure 3.1. Flow diagram for atomic physics and CRE modules.

levels ('config.tab' and 'autost.tab'), and one file containing user-specified parameters ('state.inp' or standard input on the IBM). An example of the user-specified input for C-like oxygen is shown in Figure 3.2. This input must be changed for each ion by changing the atomic number and/or the number of bound electrons. Output from STATE consists of two files ('config.inp' and 'hygen_cfg') which contain configuration data to be read in by ATBASE. A sample 'config.inp' file for C I is shown in Figure 3.3.

3.1.2. ATBASE

ATBASE is used to calculate atomic energy levels, wave functions, oscillator strengths, and photoionization cross sections. The input to ATBASE consists of four files. The file 'atbase.inp' is the calculation controller. It tells the code what calculations to do and how the calculations are to be done, such as whether to include magnetic dipole allowed oscillator strengths, how to scale energy matrix elements, and so forth. The file 'config.inp' specifies the atomic number of the ion, the number of bound electrons for the ion, and the electron configurations which are to be included in the calculation. 'hygen_cfg' contains the configurations of hydrogenic levels. Both 'config.inp' and 'hygen_cfg' are created by STATE. For isoelectronic systems with bound electron numbers larger than 22, 'config.inp' and 'hygen_cfg' need to be typed manually. 'cfp.tab' is a data file which contains the fractional parentage coefficients (FPC) for p(n), d(n) and f(n) equivalent electron groups. The important output files include:

ev_nl.dat
fv_nl.dat
ev_nl.table ⟵ configuration structure
fv_nl.table

ev_ls.dat
fv_ls.dat
ev_ls.table ⟵ LS term structure
fv_ls.table

ev_final.dat
fv_final.dat
ev_final.tab ⟵ fine structure
fv_final.tab

photoionization_x ⟵ photoionization cross sections

levels ('config.tab' and 'autost.tab'), and one file containing user-specified parameters ('state.inp' or standard input on the IBM). An example of the user-specified input for C-like oxygen is shown in Figure 3.2. This input must be changed for each ion by changing the atomic number and/or the number of bound electrons. Output from STATE consists of two files ('config.inp' and 'hygen_cfg') which contain configuration data to be read in by ATBASE. A sample 'config.inp' file for C I is shown in Figure 3.3.

3.1.2. ATBASE

ATBASE is used to calculate atomic energy levels, wave functions, oscillator strengths, and photoionization cross sections. The input to ATBASE consists of four files. The file 'atbase.inp' is the calculation controller. It tells the code what calculations to do and how the calculations are to be done, such as whether to include magnetic dipole allowed oscillator strengths, how to scale energy matrix elements, and so forth. The file 'config.inp' specifies the atomic number of the ion, the number of bound electrons for the ion, and the electron configurations which are to be included in the calculation. 'hygen_cfg' contains the configurations of hydrogenic levels. Both 'config.inp' and 'hygen_cfg' are created by STATE. For isoelectronic systems with bound electron numbers larger than 22, 'config.inp' and 'hygen_cfg' need to be typed manually. 'cfp.tab' is a data file which contains the fractional parentage coefficients (FPC) for p(n), d(n) and f(n) equivalent electron groups. The important output files include:

ev_nl.dat	
fv_nl.dat	
ev_nl.table	⟵ configuration structure
fv_nl.table	
ev_ls.dat	
fv_ls.dat	
ev_ls.table	⟵ LS term structure
fv_ls.table	
ev_final.dat	
fv_final.dat	
ev_final.tab	⟵ fine structure
fv_final.tab	
photoionization_x	⟵ photoionization cross sections

(Example for C-like Oxygen)

ATOMIC NUMBER :	8
NUMBER OF BOUND ELECTRONS:	6
THERMAL SPECTRUM (1) OR K ALPHA SPECTRUM (2):	2
MAXIMUM PRINCIPAL QUANTUM NUMBER OF THE LEVELS:	10
PRINCIPAL QUANTUM NUMBER ABOVE WHICH LEVEL STRUCTURE BECOMES HYDROGENIC:	4
PRINCIPAL (N) AND ORBITAL (L) QUANTUM NUMBER ABOVE WHICH LEVEL STRUCTURE BECOMES LS DEGENERATE:	0,0
LEVEL STRUCTURE: 1 = CONFIGURATION, 2 = TERM/FINE ST.:	2

Figure 3.2. Sample 'state.inp' file for C-like oxygen.

```
6
atomic number Z
0
net charge of the ion
1 0 0
structure index:1 or 3; fine structure boundary(n,l)


1 1 3  1002  2002  2102
CI index; output index; shell number; configuration (1000*n+100*l+e)
0 0 0
calculation control parameters (set to 0)
1 1 3  1002  2000  2104

0 0 0

1 2 4  1002  2001  2102  3201

0 0 0

2 1 3  1002  2001  2103

0 0 0

2 1 4  1002  2002  2101  3201

0 0 0
```

Figure 3.3. Sample 'config.inp' file for neutral carbon.

All the '.dat files' and the 'photoionization_x' file are data files in the formats that ATTABLE can read, while all the .table files are in the formats for viewing. Depending on what structure one is interested in, one should assign the corresponding data files with names that ATTABLE can understand. These file names are designated as

N.lev	for energy levels,
N.fda	for oscillator strengths,
N.pda	for photoionization cross sections,

where N is the number of bound electrons. For example, for an Al II system, if one is interested in the LS term structure, one should save the following files:

ev_ls.dat	====>	12.lev
fv_ls.dat	====>	12.fda
photoionization_x	====>	12.pda.

3.1.3. ATTABLE

With the raw data provided by ATBASE, the ATTABLE code can be used to create a usable 'atomic model' — an atomic data table for CRE (or KATACO-CRE). ATTABLE requires two control files and 3× NZ (where NZ = number of ions which one wants to include in the atomic model) raw data files as input:

attable.inp	
levels.inp	
N.lev	for each ion
N.fda	for each ion
N.pda	for each ion.

The file 'attable.inp' is used to specify the problem. It specifies the atomic number, number of ions to be included, and temperature and density meshes. 'levels.inp' is used to select the atomic energy levels for each ion. N.lev is a data file that contains atomic level structure data for the ion with N bound electrons, N.fda is a data file that contains oscillator strengths, and N.pda contains photoionzation cross sections. The output of ATTABLE includes two files: 'atomic.dat' and 'pixfit.dat'. The file 'atomic.dat' is an atomic data table which CRE code can read. And 'pixfit.dat' is a data file contains the fitting parameters for photoionzation cross sections.

3.1.4. CPSSR (Plane Wave Born Approximation Code)

To this point, we have described how to generate an atomic model for most applications without external ion beam effects. If one wants to include ion beam ionization effects in the spectral calculations, it is necessary to run CPSSR to get ion impact ionization cross sections and add them manually to 'rt.inp'. CPSSR requires one input file, 'cpssr.inp', and generates two output files: 'Xsecton.dat', which provides cross sections as a function of incident particle energy, and 'debug.out'. A sample input file is shown in Figure 3.4.

3.2. Standalone CRE Code

The standalone CRE code requires a namelist input file ('rt.inp') and 2 files for each plasma species ('rt.atom.dat.NN' and 'pixsec.dat.NN', where NN is the atomic number of the species). Thus, for a calculation involving an N-component plasma, 2N + 1 input files are required. The 2N atomic data files are generated using the atomic data calculation package described above. The user must supply the namelist input file. A flow diagram of the input/output files is shown in Figure 3.5.

The main output from the CRE calculation is written to 'rt.out'. This file contains information on the parameters used in the calculations, the convergence of the solution for the non-LTE populations, the distribution of atomic level populations and ionization fractions throughout the plasma, and radiation properties. The primary files used for plotting are designated 'rt.plot.NN'. These files are written from the subroutines –spect1–, –spect2–, or –spect3–, depending on the radiation transport model used. The plot files for the spectral flux emitted by the plasma is 'rt.plot.08', while that for the frequency-dependent optical depth is 'rt.plot.09'. The format of these files is of the form:

column	rt.plot.08	rt.plot.09
column 1	photon energy	photon energy
column 2	total flux	total optical depth
column 3	free-free flux	free-free optical depth
column 4	bound-free flux	bound-free optical depth
column 5	bound-bound flux	bound-bound optical depth
column 6	blackbody flux	

The photon energies are in units of eV, while the fluxes are in units of erg/cm^2/s/eV. The optical depths are of course dimensionless. The blackbody flux in

```
*
* ************************************************************
*                      NAMELIST INPUT FILE
*                            FOR
*         ION IMPACT IONIZATION CROSS SECTION CALCULATION
*                 (plane-wave-Born model + CPSSR)
*
* ************************************************************

 &inputii
*
* ........... (1) target atom information
*
      element='Al',              ! target ion ID
      z      = 13,               ! target nuclear charge
      nee    = 13,               ! number of bound electrons
      mass   = 27,               ! target atomic weight
*
* ........... (2) target state (electron configuration)
*           default setup for OI, AlI, ClI, ArI, and AUI
*
      shelln = 14                ! number of subshells of the configuration
      nle(1) = 1002, 2002,       ! 1s2, 2s2
      nle(3) = 2106, 3002,       ! 2p6, 3s2
      nle(5) = 3106, 3210,       ! 3p6, 3d10 ....
      nle(7) = 4002, 4106,       !
      nle(9) = 4210, 4314,       ! 1000*n + 100*l + e
      nle(11)= 5002, 5106,       !
      nle(13)= 5210, 6001        !

*
* .......... (3) ionized shell information
*
      nid =1,                     ! principal quantum # (n) of the ionized shell
      lid =0,                     ! orbital quantum #   (l) of the ionized shell
      vj  =-1 ,                   ! j value of the ionized shell (for ls coupling
*                                   ! set vj=-1)
*
* .......... (4) incident ion information
*
      massint = 4,               ! atomic weight
      zinct   = 2.0,             ! net charge
*
* .......... (5) beam energy
*
      units=2,                   ! unit of energy (1=2Ry, 2=eV)
      ekmin=500.0e3               ! minimum beam energy
      ekmax=10000.0d3,            ! maximum beam energy
*
*
* .......... (6) calculation  parameter

      lspdf =4,                  ! # of partial wave included (suggestion value=4)
      kepoit=20,                  ! energy mesh point used for the calculation
      seedbg=1,                   ! debug switch: 1=on, 0=off
*
*
* ......... (7) control switches

      contrl(1)=1,               ! contrl(1): binding & polarization effects (0=no,1=yes)
      contrl(2)=1,               ! contrl(2): Coulomb Deflection effect      (0=no,1=yes)
      contrl(3)=1                ! contrl(3): relativistic corrections       (0=no,1=yes)

  &end
```

Figure 3.4. Sample 'cpssr.inp' file for neutral aluminum.

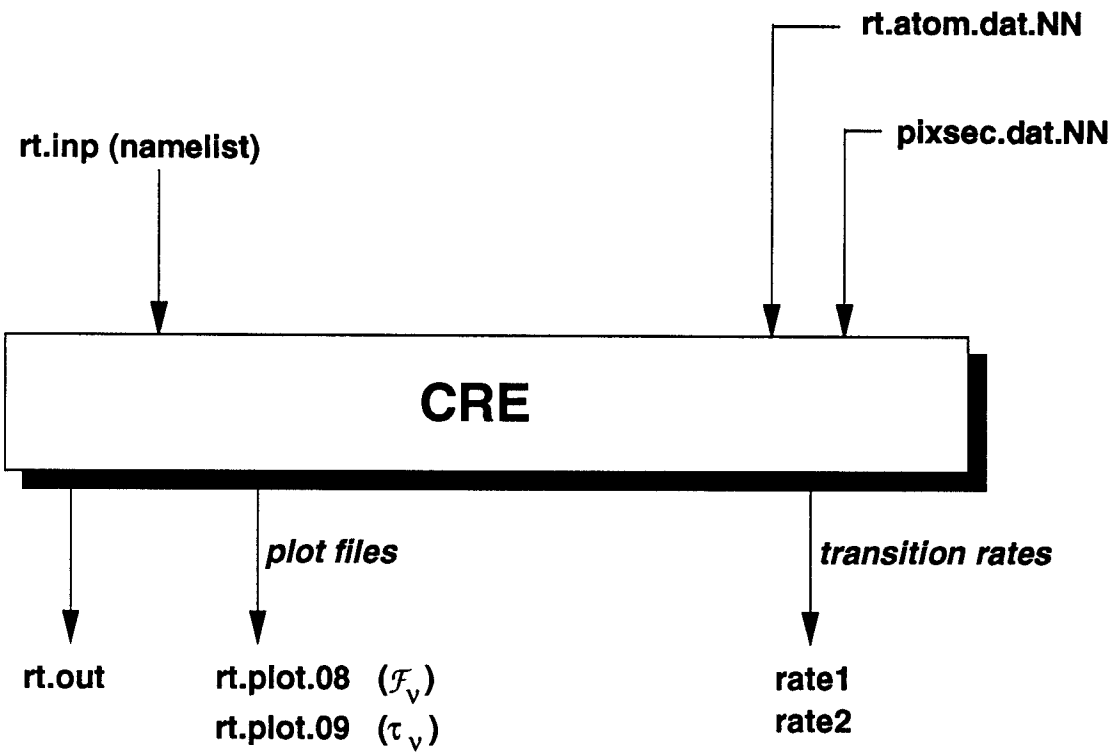

Figure 3.5. Diagram illustrating CRE input/output files.

column 6 of the flux file is based on the temperature of the outermost spatial zone. The user can also specify that the $\log_{10}$ values of the plot data be written by using the "iplot" parameter (see below).

Information on transition rates is given in the files 'rate1' and 'rate2'. This is useful when it is important to know the most important transitions which influence various atomic levels. Transition rates ($\log_{10}$ values) are written for each of the collisional and radiative processes considered along with the indices of the upper and lower levels of the transition. These results are written by subroutine –pcheck–.

We now describe how to set up the namelist input file. A list of parameters that can be read in by namelist input is given in Table 3.1. The most important items that need to be defined are the following:

- plasma properties and spatial gridding
- atomic model parameters
- spectral calculation parameters
- ion beam impact ionization rates (if a K_α calculation)
- radiation transport parameters.

An example input file is shown in Figure 3.6. In this case the plasma geometry is planar with 10 spatial zones. DRADMN defines the zone width at the plasma boundaries. The remaining zone widths are set up automatically in subroutine –zoner–. The electron temperature is 10 eV in each zone and the ion density is $6.4 \times 10^{20}\,\mathrm{cm}^{-3}$. The plasma is composed of oxygen. The first index in the "iselect" array corresponds to the atomic level index for the ground state of each ion (which is determined by looking in the file 'rt.atom.dat.08'). The proton impact ionization transition rates are taken to be 8.3×10^5 transitions/s/target ion for O I through O VII. This rate is determined from the formula:

$$R = 6.242\,\frac{P_B(\mathrm{TW/cm^2})}{E_B(\mathrm{MeV})}\,\sigma(\mathrm{barns})\,,$$

```
 $input1
c ...                                  Plasma and Grid Parameters
c                                      -------------------------
    igeom = 1
    nzones = 10
    radmin = 0.
    radmax = 1.e-3
    dradmn = 1.e-4
c ...                                  grid electron temperatures and ion densities
    tempel(1) = 10*10.,
    densnn(1) = 10*6.4e20
c ...                                  Atomic Model Parameters
c                                      ----------------------
c ...                                  atomic data parameters
    ngases = 1
    atomnm = 8.,
    atomwt = 16.
    ireada(1) = 2
c ...                                  (exc.d states to n=3)
    iselct(  1,1)  = 30*1
    iselct(134,1)  = 80*1
    iselct(257,1)  = 77*1
    iselct(334,1)  = 57*1
    iselct(391,1)  = 35*1
    iselct(426,1)  = 40*1
    iselct(466,1)  = 18*1
    iselct(484,1)  = 4*1
    iselct(494,1)  = 1
c ...                                  Proton Impact Ionization Parameters
c                                      ----------------------------------
c ...                                  consider ion-impact iz if isw37=1
    isw(37) = 1
c ...                                  proton impact ioniz. rate (trans/sec/ion)
c                                      PIMPIN(izon,isubsh,ishell,istage,igas)
    pimpin(1,1,1,1,1) = 10*8.3e5
    pimpin(1,1,1,2,1) = 10*8.3e5
    pimpin(1,1,1,3,1) = 10*8.3e5
    pimpin(1,1,1,4,1) = 10*8.3e5
    pimpin(1,1,1,5,1) = 10*8.3e5
    pimpin(1,1,1,6,1) = 10*8.3e5
c ...                                  Radiative Transfer Parameters
c                                      -----------------------------
    ilinep = 3
c ...                                  thick (isw7=0) or thin (isw7=1) for b-b
c ...                                  thick (isw8=0) or thin (isw8=1) for b-f
    isw(7)  = 1,  1,
c ...                                  if isw5=1, use multifreq. RT model
    isw(5) = 0
c ...                                  Spectral Calculation Parameters
c                                      ------------------------------
c ...                                  plot file switch (=2 for log-log plots)
    iplot(1)  = 1
    iplot(8)  = 1, 2,
c ...                                  spectral grid parameters (energies in eV)
    hvmin =  0.40e3
    hvmax =  0.75e3
    nfrqbb = 5
    nfrqff = 700
c ...                                  Miscellaneous Parameters
c                                      ------------------------
c ...                                  convergence parameters
    imaxse = 40
    errmxf = 1.e-3
c ...                                  diagonal (isw3=1) or full (isw3=0) lambda operator
    isw(3) = 1
c ...                                  isw30=1=> use gbar(Stark)=0.2
    isw(30) = 1
c ...
     con(57) = 1.0
     con(58) = 10.
c ...                                  isw34=1=> use scaling procedure to improve
c                                                condition number of matrix
     isw(34) = 1
     con(12) = 0.7
 $end
```

Figure 3.6. Sample 'rt.inp' file for standalone CRE code.

Table 3.1. Namelist Input for CRE Code

Plasma, grid parameters

IGEOM	–	Coordinate index (1 – planar, 2 – cylindrical, 3 – spherical)
NZONES	–	Number of spatial zones
RADMIN	–	Minimum radius or position (cm)
RADMAX	–	Maximum radius or position (cm)
DRADMN	–	Width of zone nearest the plasma boundary (cm)
DENSNN	–	Total ion density (number/cm^3) [array of size NZONES]
TEMPEL	–	Electron temperature (eV) [array of size NZONES]

Atomic model parameters

NGASES	–	Number of gas species
ATOMNM	–	Atomic number [array of size NGASES]
ATOMWT	–	Atomic weight [array of size NGASES]
IREAD2	–	Index to specify format of atomic data files (set equal to 2) [array of size NGASES]
FRACSP	–	fractional concentration of gases in each zone [array of size (NZONES, NGASES)] Example for homogeneous binary plasma with 20 zones: FRACSP(1,1) = 20*0.5 FRACSP(1,2) = 20*0.5 Example for layered plasma: FRACSP(1,1) = 10*1., 10*0. FRACSP(1,2) = 10*0., 10*1.
ISELCT	–	Array to select atomic levels from atomic data files 1 ⇒ on (or select); 0 ⇒ off (default) [array of size (NLEVLI, NGASES), where NLEVLI is the number of levels in the atomic data file]

Table 3.1. (continued)

Spectral calculation parameters

IPLOT	–	Select as follows IPLOT (1) = 1: compute spectral flux using escape probability radiative transfer model IPLOT (1) = 2: compute spectral flux using multi-angle, multi-frequency radiative transfer model IPLOT (1) = 3: compute spectral intensity along a specified line of sight defined by XMULOS using multi-angle, multi-frequency radiative transfer model IPLOT (8) = 1: print out photon energies and fluxes IPLOT (8) = 2: print out $\log_{10}$ values of photon energies and fluxes IPLOT (9) = 1: print out photon energies and optical depths IPLOT (9) = 2: print out $\log_{10}$ values of photon energies and optical depths
NFRQFF	–	number of frequency points for continuum
NFRQBB	–	number of frequency points for each line
HVMIN	–	minimum frequency for spectral grid
HVMIN	–	maximum frequency for spectral grid
XMULOS	–	cosine of angle used for line of sight if IPLOT (1) = 3

Radiative Transfer Parameters

ILINEP	–	line profile type (1 ⇒ Doppler; 2 ⇒ Lorentz; 3 ⇒ Voigt)
ISW (7)	–	compute photoexcitation if equal to 1
ISW (8)	–	compute photoionization if equal to 1
ISW (5)	–	if 0, use escape probability model for photoexcitation calculation if 1, use multi-angle, multi-frequency model for photoexcitation calculation
ISW (4)	–	if 0, use escape probability model for photoionization calculation if 1, use multi-angle, multi-frequency model for photoionization calculation
NFLINE	–	number of frequency points for each line
NFPIZ0	–	number of frequency points for each bound-free transition
NFCORE	–	number of frequency points in core of line (for Voigt line profiles)
BWCORE	–	bandwidth of line cores (in Doppler widths)
NANGLE	–	number of angles
NCRAD	–	number of impact parameter rays inside core (for spherical plasma with RADMIN > 0)

Table 3.1. (continued)

Ion Beam Ionization Parameters

ISW (37)	–	if 1, consider ion impact ionization
PIMPIN	–	ion beam impact ionization rate coefficient (transitions/ion/s) [array of size (NZONES, subshell number, shell number, ionization stage, NGASES). For K_α calculations, the shell and subshell indices = 1.]

Other Parameters

CON	–	Array of constants
ISW	–	Array of integer switches
IEDIT	–	Array of edit (debugging) flags
IBENCH	–	Array used for benchmark test calculations
ERRMXF	–	Maximum error allowed in fractional populations during convergence procedure
IMAXSE	–	Maximum number of iterations during convergence procedure

---

where P_B and E_B are the proton beam power density and energy, respectively. The proton impact ionization cross section, σ, is computed using the CPSSR (PWBA) code.

Regarding the radiative transfer parameters in this example, the line profiles are assumed to be Voigt. Photoexcitation and photoionization effects on the atomic level populations are not considered. This tends to be a good approximation for plasmas at low temperatures and high densities, and results in a significant savings in computational time when a large number of atomic levels and lines are considered. To test the validity of such an approximation one can simply set ISW(7) and ISW(8) to zero and compare results.

The spectrum is computed over the K-shell satellite spectral region from 0.4 to 0.75 keV. Other parameters of interest include ISW(3) and ISW(30). Setting ISW(3) = 1 uses the "diagonalized Λ-operator" procedure. This should be used for laboratory plasmas. When ISW(30) = 1, the $\bar{g}$ parameter used in computing Stark-broadened line widths is assumed to have a value of 0.2. This again can result in significant computational savings when a large number of lines is considered.

Definitions of the ISW and CON parameters are printed in the output. A more comprehensive description of the use of the CRE code will be provided in the future.

A partial listing of the output from a calculation similar to that described above is shown in Figure 3.7. Shown are the position-dependent populations for the first 80 levels (other levels not shown here) and ionization fractions. (The correspondence between atomic level and level index is also printly explicity in the output file.) These portions of the output file and the plot files 'rt.plot.08' and 'rt.plot.09' should generally be of greatest interest to the user.

3.3. KATACO-CRE Coupling

Major portions of the CRE code have been coupled to KATACO to allow for a more accurate treatment of line radiation transport. The coupling has been implemented as follows. The plasma energy equation for each spatial zone can be written as:

$$De/Dt = -D(u^2/2)/Dt + \rho^{-1}\nabla \cdot (pu) - J + A + S \tag{3.1}$$

where e is the plasma specific internal energy, u is the fluid velocity, p is the pressure, ρ is the density, A and J are the radiation absorption and emission terms, and S is a source term (which includes, for example, ion beam energy deposition). Thus, the internal energy at time t_{n+1} is given by:

$$e(t_{n+1}) = e(t_n) + (t_{n+1} - t_n)De/Dt\,. \tag{3.2}$$

The various contributions to De/Dt are evaluated using the plasma conditions at t_n. This form of time stepping is first order accurate in time. This approach has been applied successfully by others in a wide variety of studies (Clark and Apruzese, 1991).

In KATACO-CRE, the temperature distribution is computed from the solution of the plasma energy equation. Continuum radiation is transported using a multi-group radiation diffusion model. The transport of line radiation is accomplished using the CRE model. Given the plasma temperature at time t_n, one computes the atomic level populations and electron densities for each zone using the non-LTE radiative transfer/CRE model.

Once $T(r), n_e(r)$, and the atomic level populations are known, the radiation emission and absorption rates are easily computed from the zone-to-zone coupling coefficients, Q^{ea}. The emission rate in zone d due to all bound-bound transitions can

POPULATIONS vs. POSITION: Fractional Populations wrt Species Total for Gas # 1:

r (cm) fractional populations for levels 1 through 10:
5.00000E-05 2.96E-04 1.39E-04 1.42E-04 8.09E-05 2.39E-05 4.93E-04 2.96E-04 2.91E-04 9.91E-05 1.42E-04
3.00000E-04 2.96E-04 1.39E-04 1.42E-04 8.09E-05 2.39E-05 4.93E-04 2.96E-04 2.91E-04 9.91E-05 1.42E-04
7.00000E-04 2.96E-04 1.39E-04 1.42E-04 8.09E-05 2.39E-05 4.93E-04 2.96E-04 2.91E-04 9.91E-05 1.42E-04
9.50000E-04 2.96E-04 1.39E-04 1.42E-04 8.09E-05 2.39E-05 4.93E-04 2.96E-04 2.91E-04 9.91E-05 1.42E-04
r (cm) fractional populations for levels 11 through 20:
5.00000E-05 4.84E-05 1.30E-04 1.54E-05 3.01E-04 2.15E-04 3.86E-04 1.30E-04 4.39E-05 4.40E-05 7.27E-05
3.00000E-04 4.84E-05 1.30E-04 1.54E-05 3.01E-04 2.15E-04 3.86E-04 1.30E-04 4.39E-05 4.40E-05 7.27E-05
7.00000E-04 4.84E-05 1.30E-04 1.54E-05 3.01E-04 2.15E-04 3.86E-04 1.30E-04 4.39E-05 4.40E-05 7.27E-05
9.50000E-04 4.84E-05 1.30E-04 1.54E-05 3.01E-04 2.15E-04 3.86E-04 1.30E-04 4.39E-05 4.40E-05 7.27E-05
r (cm) fractional populations for levels 21 through 30:
5.00000E-05 1.01E-04 6.69E-05 4.00E-05 1.05E-04 2.43E-04 5.86E-05 1.74E-04 8.17E-05 3.56E-05 1.06E-04
3.00000E-04 1.01E-04 6.69E-05 4.00E-05 1.05E-04 2.43E-04 5.86E-05 1.74E-04 8.17E-05 3.56E-05 1.06E-04
7.00000E-04 1.01E-04 6.69E-05 4.00E-05 1.05E-04 2.43E-04 5.86E-05 1.74E-04 8.17E-05 3.56E-05 1.06E-04
9.50000E-04 1.01E-04 6.69E-05 4.00E-05 1.05E-04 2.43E-04 5.86E-05 1.74E-04 8.17E-05 3.56E-05 1.06E-04
r (cm) fractional populations for levels 31 through 40:
5.00000E-05 6.22E-03 1.12E-02 5.98E-03 3.97E-03 1.79E-03 1.74E-03 8.37E-04 2.64E-04 2.31E-04 1.13E-03
3.00000E-04 6.22E-03 1.12E-02 5.98E-03 3.97E-03 1.79E-03 1.74E-03 8.37E-04 2.64E-04 2.31E-04 1.13E-03
7.00000E-04 6.22E-03 1.12E-02 5.98E-03 3.97E-03 1.79E-03 1.74E-03 8.37E-04 2.64E-04 2.31E-04 1.13E-03
9.50000E-04 6.22E-03 1.12E-02 5.98E-03 3.97E-03 1.79E-03 1.74E-03 8.37E-04 2.64E-04 2.31E-04 1.13E-03
r (cm) fractional populations for levels 41 through 50:
5.00000E-05 2.23E-03 1.32E-03 1.05E-03 6.09E-04 4.01E-04 5.97E-04 1.21E-03 2.29E-03 8.17E-04 9.73E-04
3.00000E-04 2.23E-03 1.32E-03 1.05E-03 6.09E-04 4.01E-04 5.97E-04 1.21E-03 2.29E-03 8.17E-04 9.73E-04
7.00000E-04 2.23E-03 1.32E-03 1.05E-03 6.09E-04 4.01E-04 5.97E-04 1.21E-03 2.29E-03 8.17E-04 9.73E-04
9.50000E-04 2.23E-03 1.32E-03 1.05E-03 6.09E-04 4.01E-04 5.97E-04 1.21E-03 2.29E-03 8.17E-04 9.73E-04
r (cm) fractional populations for levels 51 through 60:
5.00000E-05 1.62E-03 1.13E-03 4.83E-04 7.94E-04 1.63E-04 4.75E-04 9.06E-04 1.15E-03 6.36E-04 3.80E-04
3.00000E-04 1.62E-03 1.13E-03 4.83E-04 7.94E-04 1.63E-04 4.75E-04 9.06E-04 1.15E-03 6.36E-04 3.80E-04
7.00000E-04 1.62E-03 1.13E-03 4.83E-04 7.94E-04 1.63E-04 4.75E-04 9.06E-04 1.15E-03 6.36E-04 3.80E-04
9.50000E-04 1.62E-03 1.13E-03 4.83E-04 7.94E-04 1.63E-04 4.75E-04 9.06E-04 1.15E-03 6.36E-04 3.80E-04
r (cm) fractional populations for levels 61 through 70:
5.00000E-05 1.24E-04 3.66E-04 1.68E-02 2.32E-02 3.13E-02 4.09E-02 7.29E-03 5.20E-02 4.62E-04 6.47E-02
3.00000E-04 1.24E-04 3.66E-04 1.68E-02 2.32E-02 3.13E-02 4.09E-02 7.29E-03 5.20E-02 4.62E-04 6.47E-02
7.00000E-04 1.24E-04 3.66E-04 1.68E-02 2.32E-02 3.13E-02 4.09E-02 7.29E-03 5.20E-02 4.62E-04 6.47E-02
9.50000E-04 1.24E-04 3.66E-04 1.68E-02 2.32E-02 3.13E-02 4.09E-02 7.29E-03 5.20E-02 4.62E-04 6.47E-02
r (cm) fractional populations for levels 71 through 80:
5.00000E-05 7.88E-02 1.01E-02 1.36E-02 1.77E-02 2.26E-02 2.81E-02 3.42E-02 1.10E-03 1.52E-03 2.04E-03
3.00000E-04 7.88E-02 1.01E-02 1.36E-02 1.77E-02 2.26E-02 2.81E-02 3.42E-02 1.10E-03 1.52E-03 2.04E-03
7.00000E-04 7.88E-02 1.01E-02 1.36E-02 1.77E-02 2.26E-02 2.81E-02 3.42E-02 1.10E-03 1.52E-03 2.04E-03
9.50000E-04 7.88E-02 1.01E-02 1.36E-02 1.77E-02 2.26E-02 2.81E-02 3.42E-02 1.10E-03 1.52E-03 2.04E-03

IONIZATION DISTRIBUTIONS IN EACH ZONE:

Zone index	electron density	Ionization Stage: 1	2	3	4	5	6	7	8	9
1	1.014E+21	.0044	.5150	.3750	.1024	.0031	.0000	.0000	.0000	.0000
2	1.014E+21	.0044	.5150	.3750	.1024	.0031	.0000	.0000	.0000	.0000
3	1.014E+21	.0044	.5150	.3750	.1024	.0031	.0000	.0000	.0000	.0000
4	1.014E+21	.0044	.5150	.3750	.1024	.0031	.0000	.0000	.0000	.0000

Figure 3.7. Partial listing of sample 'rt.out' file.

be written as:

$$J_d = \sum_{u>\ell} \Delta E_{u\ell}\, A_{u\ell}\, n_u^d \tag{3.3}$$

where $A_{u\ell}$ is the spontaneous emissison rate for the transition $u \rightarrow \ell$, $\Delta E_{u\ell}$ is the transition energy, and n_u^d is the number density of atoms in the upper state of the transition in zone d. To determine the absorption rate for zone d, we add the contribution of photons emitted in each zone:

$$A^d = (\Delta V^d)^{-1} \sum_{u>\ell} \Delta E_{u\ell}\, A_{u\ell} \sum_e n_u^e\, \Delta V^e\, Q^{ed} \tag{3.4}$$

where ΔV^d is the volume of zone d.

The radiant energy flux escaping at the plasma boundary at each time step is computed by subtracting the absorption rate for all zones from the emission rate summed over zones:

$$F_{surface} = (Area)^{-1} \sum_{u>\ell} \Delta E_{u\ell}\, A_{u\ell} \sum_e n_u^e\, \Delta V^e\, (1 - \sum_a Q^{ea})\,. \tag{3.5}$$

3.3.1. Description of Code Use

If the CRE module is invoked, data required for the CRE calculation is read in at the beginning of the calculation. The files used are similar to those for the standalone CRE code: a namelist input file ('nltert.inp') and two atomic data files ('rt.atom.dat.NN' and 'pixsec.dat.NN'). The namelist input is used to specify the following:

- atomic model parameters
- radiation transport parameters.

Plasma properties (T, ρ) and spatial gridding are not needed as they are supplied from the hydrodynamics calculation within KATACO. At present, the spectra should be computed in a post-processing fashion using the standalone CRE code. For this reason proton impact ionization effects are not considered in the KATACO-CRE calculation. In the CRE module, proton impact ionization serves to populate autoionization states, which influences the spectrum, but the radiative energy transport associated with this is minimal. Energy transfer from the beam to the target plasma is not considered in the

CRE module. Instead, this effect is computed in the ion beam energy deposition module of KATACO.

The namelist input for the CRE parameters is essentially a subset of the standalone CRE code. The namelist variables for the atomic data and radiative transfer parameters are the same. An example namelist input file for the CRE module is shown in Figure 3.8. This example is for a carbon plasma calculation. Note that only a small number of levels is chosen ($N_L = 17$). One must of course consider the trade-offs in accuracy and computer time requirements in selecting the number of levels.

Based on recent conversations with KfK personnel, it appears that one of the first applications of KATACO-CRE will be to study plasma dynamics of the divertor region during a tokamak plasma disruption. According to our present understanding, the plasma is characterized by low temperatures ($T \lesssim 10$ eV) and moderate to high densities ($n \gtrsim 10^{18}\,\mathrm{cm}^{-3}$). For these conditions, the atomic level populations should be well-approximated by local thermodynamic equilibrium (LTE). In this case, substantial savings in computer time can be realized by neglecting all radiative processes in computing the multilevel atomic rate equations. This is presently done by setting ISW(7) and ISW(8) to 1, and CON(43), CON(46), CON(47), and CON(48) to zero. After the populations are computed the line radiation fluxes will be calculated and returned through the KATACO-CRE interface.

```
 $input1
c ...                              atomic data parameters
c                                  ---------------------
      ireada(1) = 2
      ireadp(1) = 1
      fracsp(1,1) = 100*1.,
      atomnm(1) = 6.
      atomwt(1) = 12.
c ...                              select carbon levels
      iselct(  1,1)  = 1,
      iselct( 34,1)  = 1, 0,
      iselct( 52,1)  = 1, 0, 1,
      iselct( 71,1)  = 1, 1, 1,
      iselct( 83,1)  = 1*1,
      iselct(101,1)  = 7*1,
      iselct(116,1)  = 1,
c ...                              radiative transfer parameters
c                                  ----------------------------
      ilinep = 1
c ...                              thick (isw7=0) or thin (isw7=1) plasma for bound-bound
c ...                              thick (isw8=0) or thin (isw8=1) plasma for bound-free
      isw(7)  = 0,  0,
c ...                              NLTE-RT method (isw4,5=0:=>EP; =1:=>multifreq.)[5:b-b]
      isw(4) = 0, 0,
c ...                              miscellaneous parameters
c                                  -----------------------
c ...                              multipliers for rate coefficients
c                                    con(41-43) = coll exc, coll dex, spon. em.
c                                    con(44-48) = coll iz, coll rec, rad rec, dielrc, autoiz
      con(41) = 1., 1., 1.,
      con(44) = 1., 1., 1., 1., 1.,
c ...                              ionization windowing boundaries
      con(57) = 0.7, 20.
c ...                              convergence parameters (populations)
      imaxse = 60
      errmxf = 1.e-3
c ...
      iedit(60) = 2
      iedit(70) = 2
      iedit(75) = 2
c ...
      isw(3) = 1
      isw(16) = 1
      isw(6) = 1
 $end
```

Figure 3.8. Sample namelist input file ('nltert.inp') for KATACO-CRE.

4. Diode Plasma Calculations

A series of calculations were performed to aid in the interpretation of diode plasma experiments being carried out by H. Laqua and H. Bluhm. The purpose of the calculations is to predict ionization fractions and line optical depths for carbon and hydrogen as a function of plasma conditions. To do this, we have used a collisional-radiative equilibrium code which solves *steady-state* atomic rate equations. Because the time scales in the experiment are very short ($\sim 10^{-9}$ s) and densities are moderately low ($\sim 10^{15}-10^{18}$ cm^{-3}), the steady-state approximation cannot be considered reliable. Thus, these results should be considered to be estimates as opposed to accurate predictions. The results presented here supersede those reported last year (MacFarlane, Wang, and Henderson 1992) because they are based on more accurate atomic physics models.

A series of calculations was performed for plasmas composed of 95% H and 5% C for densities ranging from $10^{16} - 10^{18}$ cm^{-3} and temperatures ranging from 1 eV to 6 eV. In these calculations photoexcitation rates were computed using an escape probability model (MacFarlane et al. 1990, 1991). For the calculation of the atomic level populations, the plasma was assumed to be an infinitely extending slab of thickness 0.1 cm. This corresponds roughly to the shortest path of escape for photons. After the populations were computed, line of sight (LOS) optical depths for various lines were calculated assuming a path length of 7 cm.

Results from the calculations are shown in Table 4.1 and Figures 4.1 through 4.5. Figures 4.1, 4.2, and 4.3 show the temperature dependence of the carbon ionization fractions at ion densities (total of H + C) of 10^{16}, 10^{17}, and 10^{18} cm^{-3}, respectively. The electron densities are given in Table 4.1, as are the line center optical depths for H_α, H_β, and C II λ6578. Over this density range, C III tends to be the dominant ionization stage at $T \simeq 3.5$ eV, while C II dominates at lower temperatures down to about 1 eV. Hydrogen (see Table 4.1) tends to be fully ionized at $T \gtrsim 2$ eV, while neutral hydrogen is the dominant species at $T \lesssim 1$ eV.

The C II λ6578 line center optical depth peaks at $\tau = 0.34$ at $T = 2$ eV when $n_e = 10^{17}$ cm^{-3}. This suggests that if at $n_e = 10^{17}$ cm^{-3} C II lines are observed but no opacity broadening effects are observed in the H_α line, then the electron temperature should be in the vicinity of 3 – 4 eV. At temperatures above this very little C II should be present while at temperatures below this H_α should exhibit some opacity broadening. Note, however, that these conclusions are based on calculations assuming steady-state

Table 4.1. Diode Plasma Calculations

			Optical Depth			Ionization Fraction*						
T(eV)	$n(\mathrm{cm}^{-3})$	$\bar{Z} = \frac{n_e}{n}$	H_α	H_β	$\lambda 6578$	HII	CI	CII	CIII	CIV	CV	CVI
1	10^{16}	0.44	0.52	.015	$< 10^{-3}$	.42	.11	.89	0	0	0	0
2	10^{16}	1.00	.084	.002	.066	.9976	0	.92	.083	0	0	0
4	10^{16}	1.06	.008	$< 10^{-3}$	.008	.9999	0	.014	.71	.27	0	0
6	10^{16}	1.10	.002	$< 10^{-3}$	$< 10^{-3}$	1	0	0	.063	.87	.071	0
1	10^{17}	0.19	3.5	.091	.001	.16	.24	.76	0	0	0	0
2	10^{17}	0.99	1.8	.049	0.34	.988	.003	.88	.12	0	0	0
4	10^{17}	1.08	0.18	.005	.018	.9996	0	.004	.39	.60	0	0
6	10^{17}	1.10	0.050	.002	$< 10^{-3}$	.9999	0	0	.019	.89	.094	0
1	10^{18}	0.071	17	0.43	.002	.049	.512	.488	0	0	0	0
2	10^{18}	0.91	34	.91	0.46	.906	.023	.951	.026	0	0	0
4	10^{18}	1.06	3.6	.11	0.18	.9968	0	.024	.74	.24	0	0
6	10^{18}	1.10	1.1	.033	.001	.9988	0	0	.044	.85	.11	0

*A value of zero indicates $\lesssim 10^{-3}$.

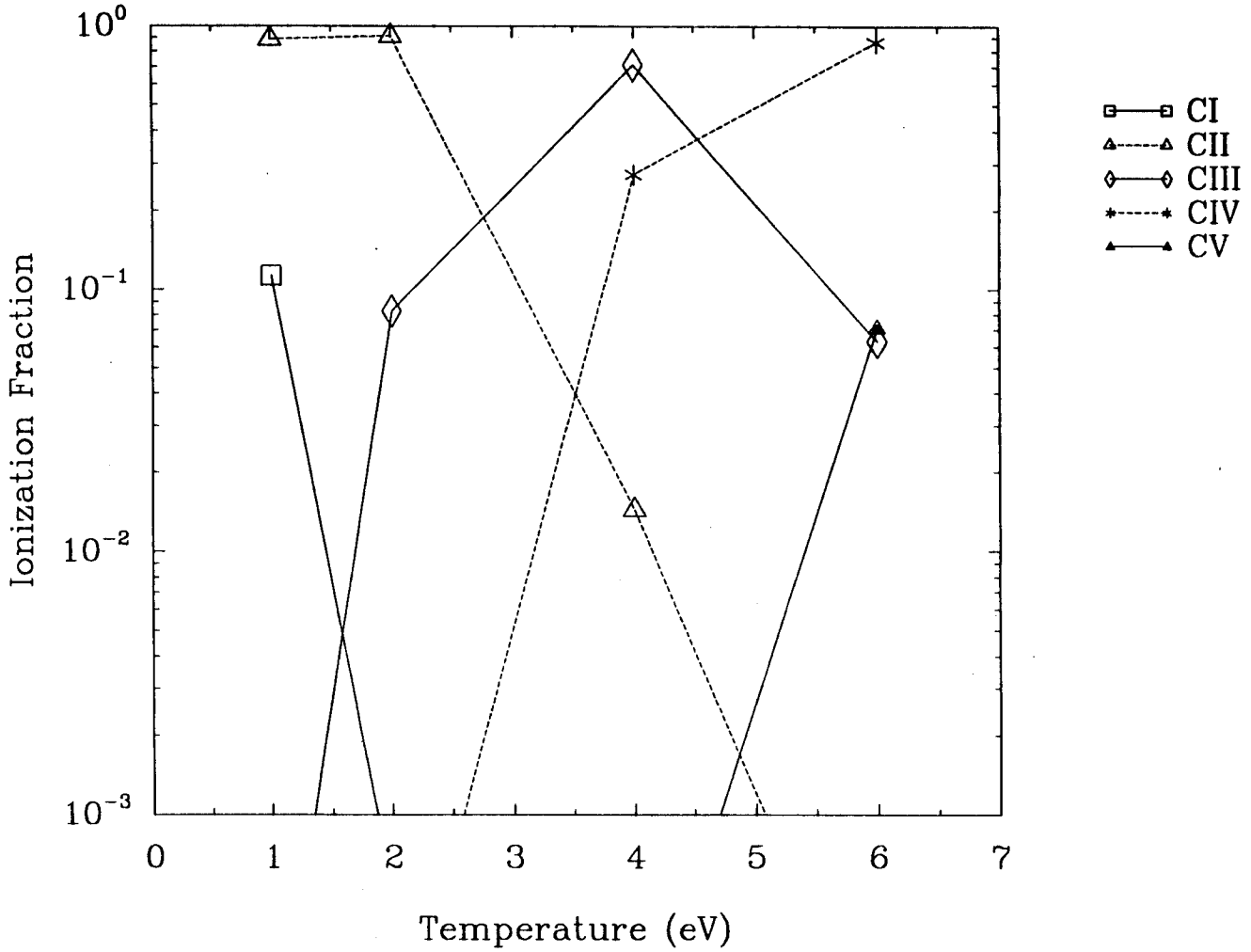

Figure 4.1. Ionization fraction of C I through C V versus temperature for a two-component plasma with $n_H = 0.95 \times 10^{16}\,\mathrm{cm}^{-3}$ and $n_C = 0.05 \times 10^{16}\,\mathrm{cm}^{-3}$.

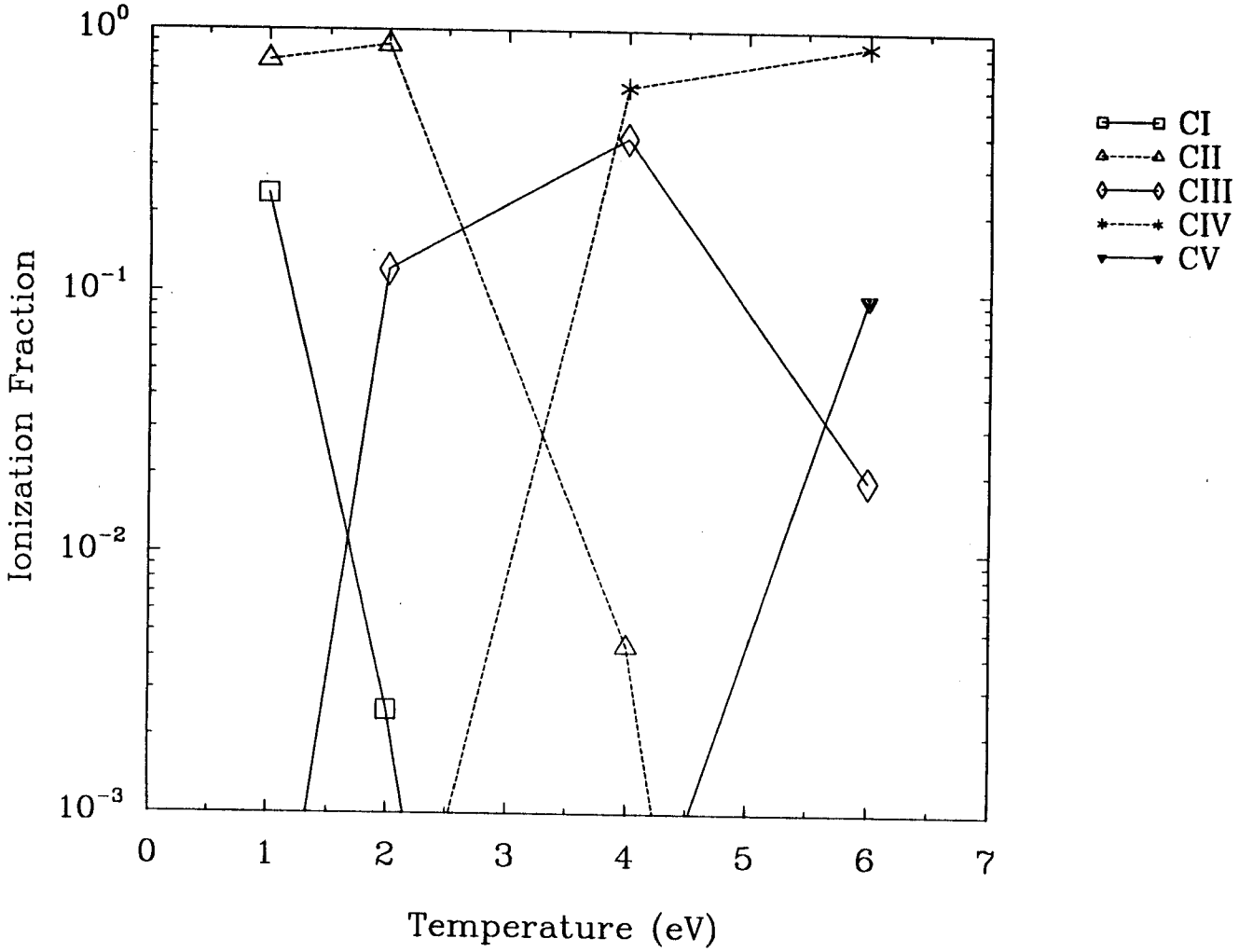

Figure 4.2. Same as Figure 4.1 but with $n_{\mathbf{total}} = 10^{17}\,\mathbf{cm^{-3}}$.

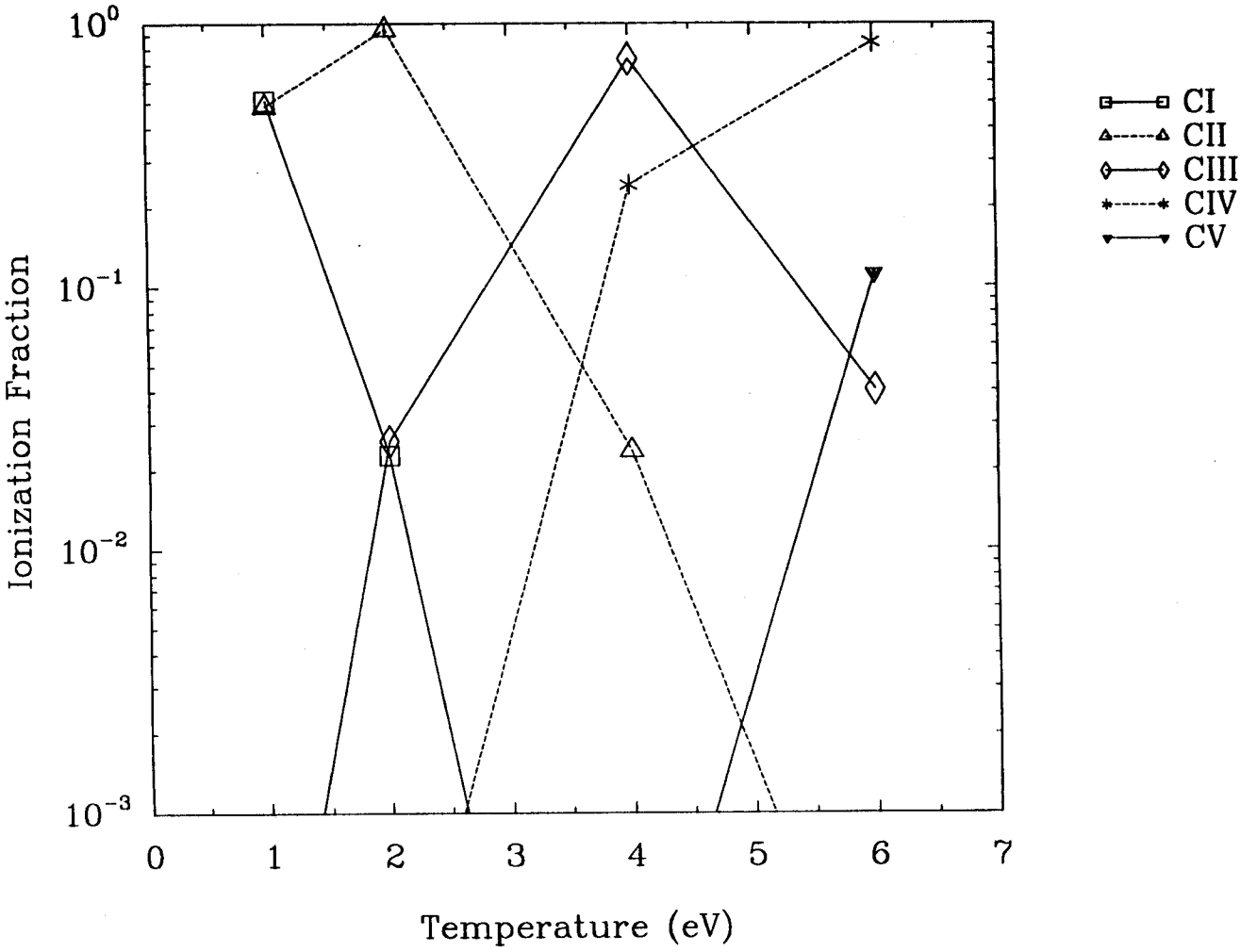

Figure 4.3. Same as Figure 4.1 but with $n_{\mathbf{total}} = 10^{18}\,\mathrm{cm}^{-3}$.

populations. If the H $n = 2$ state or C II ionization fraction is significantly altered by injection of new material at the anode surface, one should rely on an analysis based on the solution of time-dependent rate equations.

It is sometimes useful to be able to estimate line opacities from simple analytic models. We have done this for the case of hydrogen using the assumption of local thermodynamic equilibrium (LTE). At the temperatures and densities considered in this section, departures from LTE due to *radiative* processes tend not to be very significant. On the other hand, departures from LTE due to injection of material at the anode surface can be important (Maron et al. 1989). Thus, an accurate determination of line opacities may require that such time-dependent processes be considered.

Let us consider the idealized case of a pure hydrogen plasma in LTE. The ratio of the H I $n = 2$ number density, n_2, to the H II number density, n_κ, is given by the Saha equation (see, e.g., Mihalas 1978):

$$\frac{n_2}{n_\kappa} = (1.66 \times 10^{-22}\,\mathrm{cm}^3\,\mathrm{eV}^{3/2}) \left(\frac{g_2}{g_\kappa}\right) n_e\, T^{-3/2}\, e^{\Delta E_{2,\kappa}/T}\,, \tag{4.1}$$

where n_e and T are the electron density and temperature, g_2 and g_κ are the statistical weights of the $n = 2$ and continuum states, respectively, and $\Delta E_{2,\kappa}$ is the transition energy between the two states.

The population density of the upper state of the Balmer transition is obtained from Boltzmann's statistics:

$$\frac{n_u}{n_2} = \frac{g_u}{g_2}\, e^{-\Delta E_{2,u}/T}\,, \tag{4.2}$$

where the subscript u refers to the upper state. The optical depth at the center of a line can be written as

$$\tau_o = L \cdot \left(n_2 - \frac{g_2}{g_u}\, n_u\right) \left(\frac{\pi e^2}{m_e c}\right) f_{u2}\, \phi_{\nu_o}\,, \tag{4.3}$$

where L is the plasma width, f_{u2} is the oscillator strength, and ϕ_{ν_o} is the value of the profile at line center. Combining Eqs. (4.1) through (4.3) we get:

$$\tau_o = (3.5 \times 10^{-23}\,\mathrm{cm}^5\,\mathrm{s}^{-1}\,eV^{3/2})\, L\, n_e^2\, T^{-3/2}\, (1 - e^{-\Delta E_{2,u}/T})\, e^{\Delta E_{2,\kappa}/T}\, \cdot f_{ul}\, \phi_{\nu_o}\,. \tag{4.4}$$

For a Lorentzian profile with a FWHM wavelength $\Delta\lambda_{\mathrm{FWHM}}$, the value of the profile function at line center is:

$$\phi_{\nu_o} = \frac{2\lambda^2}{\pi c\, \Delta\lambda_{\mathrm{FWHM}}}\,.$$

The FWHM for hydrogen Balmer lines can be approximated by (Weise et al. 1972):

$$\Delta\lambda_{\rm FWHM} \cong \begin{cases} 9.2\,\text{Å}\,(n_e/10^{17}\text{cm}^{-3}) & \text{for} \quad \text{H}_\alpha \\ \\ 42\,\text{Å}\,(n_e/10^{17}\text{cm}^{-3}) & \text{for} \quad \text{H}_\beta\,. \end{cases}$$

Using this analysis we have calculated the H_α and H_β line center optical depths for a line of sight path length of 7 cm. The results are shown in Figures 4.4 and 4.5. A comparison of these figures with the results in Table 4.1 indicates that the LTE model and the CRE calculations produce similar results.

The primary differences between the two calculations occur at low temperatures and occur because the simple analytical model does not include the free electrons from the carbon ions. At temperatures below about 2 – 3 eV the H_α optical depths exceed unity. The H_α line center optical depths drop below 10^{-1} at temperatures of about 4.5 eV and 1.8 eV for densities of 10^{17} and 10^{16} cm^{-3}, respectively. Figure 4.5 shows the H_β lines should only exhibit opacity broadening at $T < 1.5$ eV for densities $\gtrsim 10^{17}$ cm^{-3}.

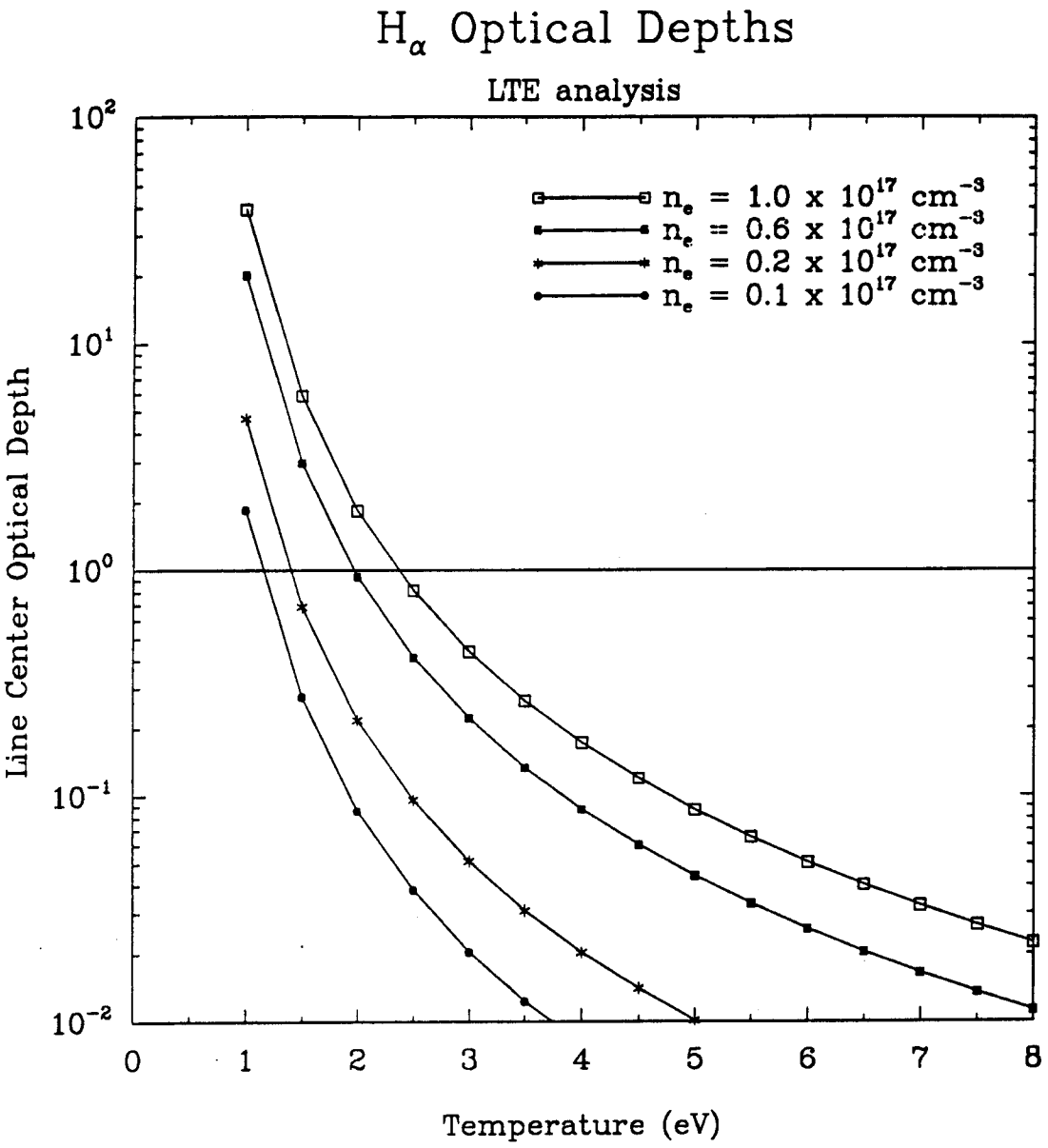

Figure 4.4. H_α line center optical depth as a function of temperature calculated from LTE analysis. The electron densities are indicated for each curve.

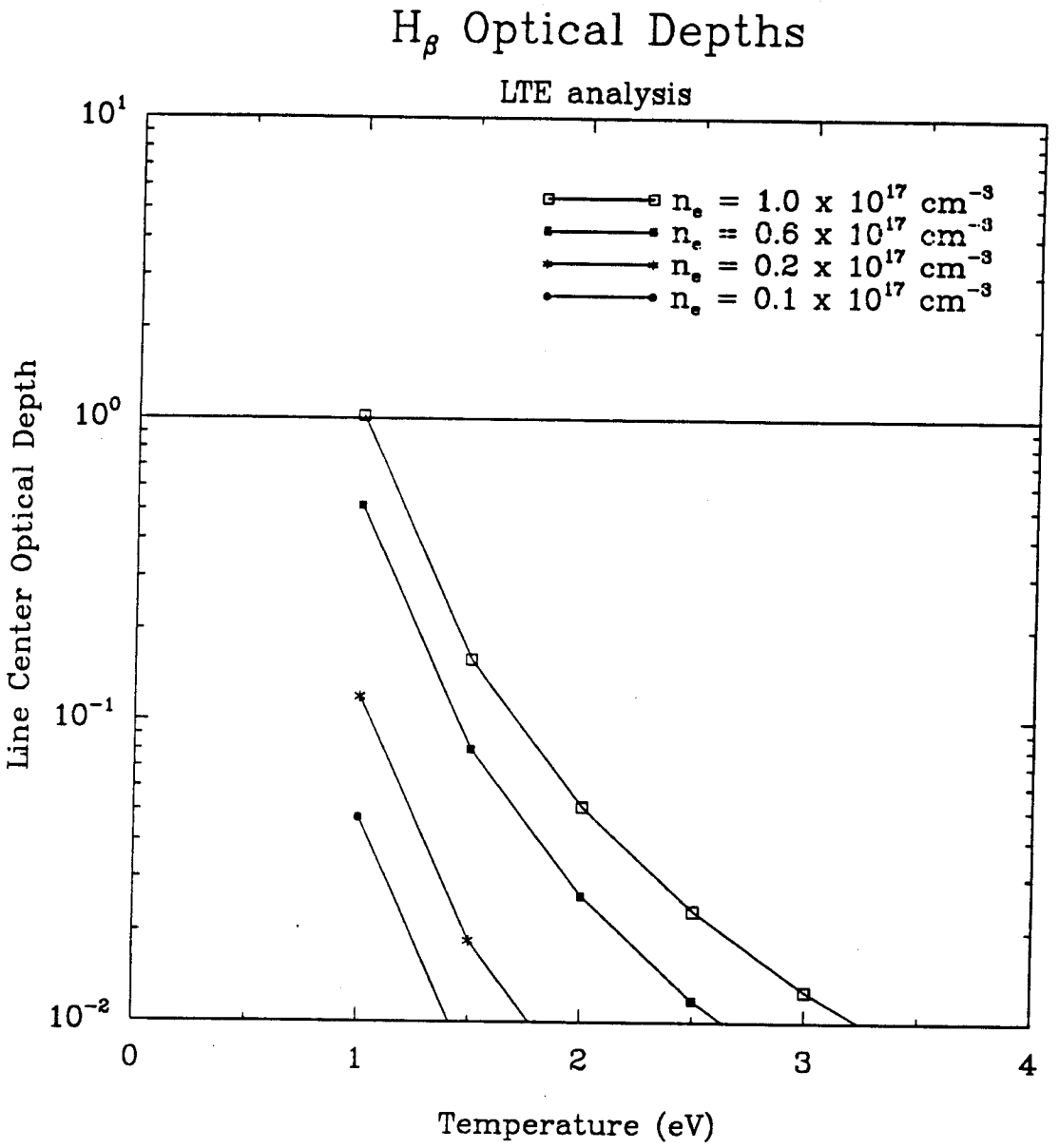

Figure 4.5. Same as Figure 4.4 but for H_β.

5. Summary

During the past year, our efforts focused on: (1) completing the coupling of the non-LTE radiative transfer (CRE) code with KATACO; (2) installation of the KATACO-CRE, standalone CRE, and the supporting atomic physics codes on the KfK computer system; and (3) performing calculations in support of KALIF experiments. In regards to the first item, we have successfully coupled the CRE algorithms into KATACO. The purpose of adding this model is to allow for a more accurate treatment of line radiation transport in problems where it can have a significant influence on the overall plasma energetics. The KATACO-CRE code was installed on the KfK IBM mainframe during J. MacFarlane's visits to KfK in September and December 1992.

We have also installed the standalone CRE code and the supporting atomic physics codes. Both codes have been successfully tested on the IBM mainframe. In addition, the atomic physics codes have been installed on the STARDENT workstation at KfK. A substantial effort was made to ensure the codes are "user friendly," although there is still more work to be done in this area. A brief description of how to use the codes appears in Section 3 of this report. We anticipate writing more detailed users' guides in the upcoming year.

Finally, we have performed several sets of calculations in support of KALIF experiments. In addition to the Al K_α temperature diagnostic calculations which are described in detail in the appendices, we have performed a series of calculations to assess the benefits of using O K_α satellite emission as a diagnostic in proton beam experiments in which targets are heated to moderate temperatures. It was shown that the O K_α spectrum exhibits good temperature sensitivity between $T = 2$ and 20 eV as satellites are discernibly blue-shifted even at the lowest ionization stages. Thin tracer layers with thicknesses $\sim 100 - 1000$ Å would be preferable in such experiments because opacity effects would be significantly reduced.

A brief set of calculations was also performed to support diode plasma experiments being performed by H. Laqua and H. Bluhm. Our results suggest that the H_α and H_β line profiles observed in these experiments are likely to be influenced by opacity effects at relatively low plasma temperatures.

Acknowledgments

The authors gratefully acknowledge support from Kernforschungszentrum Karlsruhe through Fusion Power Associates. We also thank Dr. W. Hobel and Dr. B. Goel for their very valuable assistance in installing codes on the KfK computers. Finally, we would like to express special thanks to Dr. Reimar Fröhlich, who retired at the end of 1992. We sincerely appreciate the support, hospitality, and friendship he has provided to us and our colleagues at Wisconsin over the years.

References

Abdallah, J., Clark, R.E.H., and Peek, J.M., *Phys. Rev.* **A 44**, 4072 (1991).

Bailey, J., Carlson, A.L., Chandler, G., Derzon, M.S., Dukart, R.J., Hammel, B.A., Johnson, D.J., Lockner, T.R., Maenchen, J., McGuire, E.J., Mehlhorn, T.A., Nelson, W.E., Ruggles, L.E., Stygar, W.A., and Wenger, D.F., *Lasers and Particle Beams* **8**, 555 (1990).

Clark, R.W., and Apruzese, J.P., private communication (1991).

Goel, B., private communication, Kernforschungszentrum Karlsruhe (1992).

Krause, M.O., *J. Phys. Chem. Ref. Data* **8**, 307 (1979).

MacFarlane, J.J., Wang, P., and Moses, G.A., Fusion Power Associates Report No. FPA-90-1, January 1990.

MacFarlane, J.J., Wang, P., and Henderson, D.L., Fusion Power Associates Report No. FPA-91-1, January 1991.

MacFarlane, J.J., Wang, P., and Henderson, D.L., Fusion Power Associates Report No. FPA-92-1, January 1992.

MacFarlane, J.J., Wang, P., Mehlhorn, T.A., Bailey, J., and Dukart, R.J., *Rev. Sci. Instrum* **63**, 5059 (1992).

MacFarlane, J.J., Wang, P., Bailey, J., Mehlhorn, T.A., Dukart, R.J., and Mancini, R.C., *Phys. Rev. E*, in press (1993).

Maron, Y., Sarfaty, M., Perelmutter, L., Zahavi, O., Foord, M.E., and Sarid, E., *Phys. Rev.* **40**, 3240 (1989).

Mihalas, D., Stellar Atmospheres, Second Edition (Freeman, New York, 1978).

Perry, T.S., Davidson, S.J., Serduke, F.J.D., Bach, D.R., Smith, C.C., Foster, J.M., Doyas, R.J., Ward, R.A., Iglesias, C.A., Rogers, F.J., Abdallah, J., Jr., Stewart, R.E., Kilkenny, J.D., and Lee, R.W., *Phys. Rev. Lett.* **67**, 3784 (1991).

Soom, B., private communication, Laboratory for Laser Energetics, Univ. of Rochester (1992).

Wang, P., MacFarlane, J.J., and Moses, G.A., *Rev. Sci. Instrum.* **63**, 5062 (1992).

Wang, P., MacFarlane, J.J., Moses, G.A., and Bailey, J., Proceedings of the Beams 92 Conference, Washington, DC (1992).

Wang, P., MacFarlane, J.J., and Moses, G.A., submitted to Phys. Rev. (1993).

Wiese, W.L., Kelleher, D.E., and Paquette, D.R., *Phys. Rev.* **A6**, 1132 (1972).

Appendix A

Analysis of K_α Line Emission from Aluminum Plasmas Created by Intense Proton Beams

J.J. MacFarlane, P. Wang, J. Bailey,
T.A. Mehlhorn, R.J. Dukart, R.C. Mancini

(Submitted to Physical Review)

Appendix B

Relativistic Configuration Interaction Calculations for K_α Satellite Properties of Aluminum Ions

P. Wang, J.J. MacFarlane, G.A. Moses

(Submitted to Physical Review)

Appendix C

Aluminum K-Shell Line Emissison as a Diagnostic in Light Ion Beam Fusion Experiments

J.J. MacFarlane, P. Wang,
T.A. Mehlhorn, J. Bailey, R.J. Dukart

(Presented at the 9th Topical Conference on High-Temperature Plasma Diagnostics, Santa Fe, NM, March 19921; Review of Scientific Instruments, **63** 5062 (1992).)

Appendix D

Thermal Ionization Effects on Inner-Shell Line Emission for Au Targets Heated by Intense Light Ion Beams

P. Wang, J.J. MacFarlane, G.A. Moses

(Presented at the 9th Topical Conference on High-Temperature Plasma Diagnostics, Santa Fe, NM, March 19921; Review of Scientific Instruments, **63** 5059 (1992).)

Appendix E

Theoretical Spectroscopic Analysis of Intense Ion Beam-Plasma Interaction in the PBFA-II Gas Cell

P. Wang, J.J. MacFarlane, G.A. Moses, J.E. Bailey

(Proceedings of the Beams '92 Conference, Washington, DC, 1992)